A GENERALIZED NONLINEAR LUMPED CIRCUIT MODEL FOR GUNN DIODES WHICH INCLUDES FIELD-DEPENDENT DIFFUSION EFFECTS

by

L. O. Chua and Y. W. Sing

Memorandum No. UCB/ERL M77/40

2 June 1977

ELECTRONICS RESEARCH LABORATORY

College of Engineering
University of California, Berkeley
94720

A GENERALIZED NONLINEAR LUMPED CIRCUIT MODEL FOR GUNN DIODES WHICH INCLUDES FIELD-DEPENDENT DIFFUSION EFFECTS[†]

L. O. Chua and Y. W. Sing[††]

ABSTRACT

A complete nonlinear lumped circuit model for Gunn diodes which includes the effects due to domain extinction and nucleation phenomena is presented. The model is based upon physical principles and allows an arbitrary nonlinear drift velocity curve v(E) and a nonlinear diffusion curve D(E) to be specified by the user. It is valid for simulating arbitrary Gunn-diode circuits operating in any matured high-field domain mode, or in the LSA mode. Under additional assumptions, the model simplifies to other existing models. Several computer-simulated examples of Gunn-diode circuits operating under both steady state and transient regimes are presented. Finally, a rigorous definition of a "dc" I-V curve for Gunn diodes is offered and shown to be rather useful for predicting the qualitative behavior of Gunn-diode circuits during all time intervals where a matured domain exists.

[†]Research sponsored by the Office of Naval Research Contract N00014-76-0572 and by the Miller Institute which supported the first author during the 1976-77 Academic Year as a Miller Research Professor.

[††]Department of Electrical Engineering and Computer Sciences and the Electronics Research Laboratory, University of California, Berkeley, California 94720.

I. INTRODUCTION

Gunn diodes are two-terminal "transferred-electron" devices which are finding increasing applications as a basic "low-noise" active component in the design of microwave circuits [1-4]. Our objective in this paper is to present a new nonlinear lumped circuit model which is capable of simulating the Gunn diode's various distinct operating modes; namely, the transit-time mode, the delayed-domain mode, the quenched-domain mode, and the LSA mode. Although only these four well-known modes are simulated in this paper, our model is valid under very general operating conditions and can be used to mimic other single-domain operating modes involving a Gunn diode which satisfies the stable-domain requirement $n_0 L > 10^{12}$ cm^{-2} [1].

Several nonlinear Gunn diode lumped circuit models have been proposed over the past decade [5-8]. The Carroll-Giblin model [5] is an "analog circuit" which requires different circuit parameters for mimicking different operating modes. It is therefore not suited for computer simulation. The Robrock model [6] is ideal for computer-aided-design of Gunn-diode circuits in view of its simplicity -- it contains only 4 lumped circuit elements. However, the associated element characteristics are not derived from physical governing equations, but rather from empirical data and relationships obtained from previous computer solutions of the associated partial differential equations. Consequently, as pointed out by Gunshor and Kak [7], this model violates a basic "current conservation law" and is therefore not valid in general. This discrepancy is overcome in the latest model due to Gunshor and Kak [7] who based their derivation directly on physical governing equations for both the zero and non-zero diffusion case. The Gunshor-Kak model contains 5 elements, one of them being a nonlinear controlled current source which, in the non-zero diffusion case, depends on two "space variables" x_1 and x_2 associated with the domain width. Since x_1 and x_2 are not circuit variables, only the zero-diffusion case of the Gunshor-Kak model is suited for computer-aided circuit analysis. Finally, we remark that with the exception of the Carroll-Giblin model, all other published Gunn-diode circuit models that the authors are aware of are incomplete in the sense that they can only be used to model "domain dynamics," but not the extinction and nucleation phenomena when a high-field domain reaches the anode. Such models cannot be used for automatic circuit simulation.

The model to be presented in this paper not only overcomes the objections raised in the above cited models, but also allows the diffusion coefficient to

be a nonlinear function of field intensity. In particular, our model is imbued with the following desirable features: 1) It retains the simplicity of the Robrock model. In fact, it has an identical topology and choice of circuit elements. Only the elements' characteristics are different. 2) Our model for domain dynamics is derived entirely from the physical equations governing the device and its elements bear a one-to-one correspondence to actual physical operating mechanisms. 3) In its most general form, our model includes the nonlinear effects due to the field-dependent diffusion coefficient [9]. In particular, both the electron drift velocity-vs.-field nonlinear characteristic v(E) and the diffusion-vs.-field nonlinear characteristic D(E) can be independently specified by the user. 4) Our model structure is fixed, regardless of the various additional simplifying assumptions commonly imposed on D(E). Moreover, the characteristics of only one element need be changed when additional assumptions are made on D(E). In the limiting zero-diffusion case, our model, though topologically distinct, is in fact identical to the Gunshor-Kak model in the sense that its governing circuit equations are identical. 5) The parameters associated with our model are fixed for each given device, regardless of the mode of operation or external circuits. With the exception of the "domain width" W, all other model parameters are readily determined from the device material and geometry. The parameter W is introduced in our model to mimic the capacitance associated with the high-field domain. It will be seen in the next section that unlike the Robrock or Gunshor-Kak model where the domain width is a nonlinear function of the domain voltage, we can assign an arbitrary constant value to W in our model without affecting the solution of the circuit external to the device. 7) By adding a "timing circuit" for sensing when the domain reaches the anode, our model is capable of simulating the domain nucleation and extinction phenomena automatically. In other words, our "timing-circuit augmented" model is a complete model suitable for computer simulation under any external circuitry and over any desired time interval. 8) In its most general form, our model makes only two rather reasonable assumptions:

(a) there exists a high-field domain with a single local maxima which propagates without change of shape with a "domain velocity" $v_D(t)$ from the cathode to the anode[1]

[1] All existing circuit models for Gunn diodes made the simplifying assumption that the domain velocity $v_D(t)$ is a constant. This is not true in practice because $v_D(t)$ depends on the external circuit and is generally time-dependent. Our model allows $v_D(t)$ to be computed numerically as a function of time during any computer-simulation.

b) Quasi-static Assumption: in terms of the "moving coordinates" $y \triangleq z - \int_0^t v_D(t)dt$ and $t' \triangleq t$, we have $\partial E/\partial t' = 0$ [9].

Since no other simplifying assumptions are made, our circuit model for mimicking domain dynamics is as accurate as that of solving the original device's physical equations subject to the above two assumptions. Moreover, since our model agrees in topology with the Robrock model, and includes the Gunshor-Kak model as a special case, it can be considered as a unified circuit model for Gunn diodes having a concentration-length product $n_0L > 10^{12}$ cm^{-2}. In other words, our model is valid for all single-domain operating modes except the "accumulation-layer mode" [10].

II. LUMPED CIRCUIT MODEL FOR DOMAIN DYNAMICS

Our objective in this section is to present the circuit model for simulating the formuation of a single high-field domain in a Gunn diode. We assume a one-dimensional structure as shown in Fig. 1(a) with length L, uniform cross-sectional area A, di-electric constant ε, and a uniform donor concentration n_0, where $n_0L > 10^{-12}$ cm^{-2}. This "concentration-length inequality" is necessary to support a high-field domain consisting of an accumulation layer with carrier concentration $n \geq n_0$, and a depletion layer with carrier concentration $n \leq n_0$, as shown in Fig. 1(b). The corresponding dipole-induced field distribution is shown in Fig. 1(c). Observe that Figs. 1(b) and (c) give the typical shape of n(x) and E(x) associated with a single high-field domain at one instant of time. As the domain grows in size, it propagates from the cathode (x=0) to the anode (x=L) with an instantaneous velocity $v_D(t)$. The exact shape of n(x) and E(x) at different instants of time are governed by rather complex dynamics whose instantaneous effects on the device current and voltage will be accurately simulated by our circuit model. To distinguish between the accumulation layer and the depletion layer, we will henceforth use the symbols n_a and n_d to denote the carrier concentration in the accumulation and depletion layers, respectively; namely, $n(x) = n_a(x)$ for $x_1 \leq x \leq x_3$ and $n(x) = n_d(x)$ for $x_3 \leq x \leq x_2$. Since E(x) in Fig. 1(c) is a strictly monotonic function in the two intervals $[x_1,x_3]$ and $[x_3,x_2]$, we can eliminate the space variable x and define $n_a = n_a(E)$ as a single-valued function of E over the interval $[E_0,E_m]$ corresponding to the accumulation layer. Likewise, we can define $n_d = n_d(E)$ as a single-valued

function of E over the same interval $[E_0, E_m]$ but relative to the depletion layer.

Using the above notations, we will first present the circuit model in its most general form and show how the associated model parameters and functions are determined (Section II-A). Next, we will make two simplifying assumptions and obtain two corresponding simplified circuit models (Section II-B). Both of these subsections are addressed to the circuit designers who are mainly interested in simulating microwave circuits utilizing Gunn diodes, and not so much on the physical mechanisms inside the device. Consequently, only the minimum essentials for a complete specification of the circuit model will be presented in Sections II-A and II-B. The complete derivation and justification of our model are given in Section II-C. Finally, a comparison between our model and other existing models are given in Section II-D.

A. Description of the General Model

Our most general circuit model for simulating the dynamics of a single high-field domain is given in Fig. 2, where the element parameters and characteristics are defined as follow:

1. Cathode-to-Anode Capacitance: $C_1 = \frac{\varepsilon A}{L}$ (1)

   where ε = dielectric constant, A = cross=sectional area, and L = device length.

2. Domain Capacitance: $C_2 = \frac{\varepsilon A}{W}$ (2)

   where W = average domain width $\triangleq \lim_{T\to\infty} \frac{1}{T}\int_0^T \left[x_2(t)-x_1(t)\right] dt$ (3)

3. Nonlinear Resistor R: $I_R = G(V_R) = A\, q\, n_0 v\left(\frac{V_R}{L}\right)$ (4)

   where A = cross-sectional area, q = electron charge, n_0 = donor concentration, and v(E) is the velocity-vs.-field characteristic ($E=V_R/L$).

4. Nonlinear Controlled Current Source:

The diamond-shape symbol in Fig. 2 denotes a controlled current source whose terminal current I_D at any instant of time t depends upon the instantaneous value of the two capacitor voltages $v_1(t)$ and $v_2(t)$, and the device terminal

current I(t) in accordance with the following nonlinear relationship:[2]

$$I_D = I_D(v_1,v_2,I) \triangleq C_2F(v_1,v_2) - I \tag{5}$$

where $F(v_1,v_2)$ is a single-valued function of v_1 and v_2 defined as follow:[3]

$$F(v_1,v_2) \triangleq n_0\left\{\int_{v_1/L}^{E_m}\left[\frac{v(v_1/L)-v(E)}{n_a(E)-n_0}\right]dE + \int_{v_1/L}^{E_m}\left[\frac{v(v_1/L)-v(E)}{n_0-n_d(E)}\ dE\right]\right\} \tag{6}$$

where E_m denotes the "peak" domain field (Fig. 1(c)), $n_a(E)$ denotes the carrier concentration in the accumulation layer, and $n_d(E)$ denotes the carrier concentration in the depletion layer. In the general case where the diffusion coefficient $D = D(E)$ is a nonlinear function of the field intensity E, these three yet unspecified quantities are determined for each value of (v_1,v_2) as follow:

(1) Peak-domain Field E_m

Assuming for the moment that $n_a(E)$ and $n_d(E)$ have been found, then E_m is obtained by solving the scalar nonlinear equation

$$g(E_m;v_1,v_2) = 0 \tag{7}$$

---

[2]The constant C_2 in (5) is equal to the domain capacitance $C_2 \triangleq \varepsilon A/W$ in Fig. 2. Notice that if we apply Kirchhoff current law to the lower terminal of our model, we would obtain $I = C_2\, dv_2/dt - C_2F(v_1,v_2) + I$, which upon cancellation of I and C_2 yields the simplified equation $dv_2/dt = F(v_1,v_2)$ independent of C_2. This shows that the solution of the external circuit does not depend on the value of C_2. Hence, for computational purposes, it is convenient to simply set $C_2 = 1$. However, if one is interested also to attach some physical meaning to C_2, then one could set $C_2 = \varepsilon A/W$, where W is the average domain width defined in footnote 3.

[3]The capacitor voltage $v_1 \triangleq E_0L$ can be interpreted as that component of the device terminal voltage due the uniform field E_0 outside of the domain, and the capacitor voltage $v_2 \triangleq \int_{x_1}^{x_2}[E(x)-E_0]\,dx$ can be interpreted as the remaining device terminal voltage component due to the excess field $E(x) - E_0$ over the domain from x_1 to x_2. If we let $w(t) = x_2(t) - x_1(t)$ denote the domain width at time t, then we can define the average domain width by $W \triangleq \lim_{T\to\infty}\frac{1}{T}\int_0^T[x_2(t)-x_1(t)]dt$.

where

$$\mathcal{G}(E_m;v_1,v_2) \triangleq v_2 - \frac{\varepsilon}{q}\left\{\int_{v_1/L}^{E_m}\left[\frac{E-v_1/L}{n_a(E)-n_0}\right]dE + \int_{v_1/L}^{E_m}\left[\frac{E-v_1/L}{n_0-n_d(E)}\right]dE\right\} \quad (8)$$

Observe that since E is a dummy variable of integration, for each given value of (v_1,v_2), $\mathcal{G}(E_m;v_1,v_2)$ is a nonlinear function of E_m alone. We included the two variables v_1 and v_2 as arguments of $\mathcal{G}(\cdot)$ in order to emphasize that the solution E_m of (7) depends on both v_1 and v_2; i.e., $E_m = E_m(v_1,v_2)$.

(2) Accumulation layer carrier concentration $n_a(E)$

For each given value of (v_1,v_2), $n_a(E)$ is obtained by solving the following scalar nonlinear ordinary differential equation

$$\frac{dn_a}{dE} = \mathcal{N}_a(n_a,E;v_1,v_D) \quad (9a)$$

where

$$\mathcal{N}_a(n_a,E;v_1,v_D) \triangleq \frac{n_a\left[v(E)-v_D\right]+n_0\left[v_D-v(v_1/L)\right]-(q/\varepsilon)(n_a-n_0)n_aD'(E)}{(q/\varepsilon)(n_a-n_0)D(E)} \quad (9b)$$

$$n_a(E)\Big|_{E=E_0=v_1/L} = n_0 \quad (9c)$$

$$n_a(E)\Big|_{E=E_m} = n_0 \quad (9d)$$

The symbol D'(E) in (9b) denotes the slope dD(E)/dE of the nonlinear diffusion-vs.-field characteristic and is therefore a known quantity. The parameter v_D in (9b) has been defined earlier as the "domain velocity" and will be shown in Section II-C to depend upon both v_1 and v_2. Observe that since (9a) is a scalar first order differential equation, the two boundary conditions (9c) and (9d) cannot be satisfied simultaneously for arbitrary values of v_D. Consequently, to solve for $n_a = n_a(E)$ from (9a), we must choose an appropriate value for v_D in order that (9c) and (9d) are satisfied. In other words, rather than solving an initial-value problem, we must solve a "two-point boundary-value

problem" giving both v_D and $n_a(E)$ as its solution. The reason for prescribing the above two boundary conditions can be seen from Figs. 1(b) and (c) and will be elaborated later in Section II-C. Several numerical methods can be devised to solve this two-point boundary-value problem. One such method -- the modified shooting method -- is presented in Appendix A. To emphasize that the solution $n_a(E)$ of (9a) depends upon both v_1 and E_m, we will sometime write $n_a(E) = n_a(E;v_1,E_m)$. Observe that since E_m itself depends upon v_1 and v_2, we can also say $n_a(E)$ is a function of both v_1 and v_2. Likewise, we will sometimes write the corresponding "domain velocity" v_D obtained from solving(9a) by $v_D = v_D(v_1,v_2)$.

(3) Depletion layer carrier concentration $n_d(E)$

For each given value of (v_1,v_2), $n_d(E)$ is obtained by solving the following "initial-value problem"

$$\frac{dn_d}{dE} = \mathcal{N}_d(n_d,E;v_1,v_D) \tag{10a}$$

where

$$\mathcal{N}_d(n_d,E;v_1,v_D) \triangleq \frac{n_d[v(E)-v_D]+n_0[v_D-v(v_1/L)]-(q/\varepsilon)(n_d-n_0)n_dD'(E)}{(q/\varepsilon)(n_d-n_0)D(E)} \tag{10b}$$

$$n_d(E)\Big|_{E=E_0=v_1/L} = n_0 \tag{10c}$$

$$v_D = v_D(v_1,v_2) \tag{10d}$$

Here $v_D = v_D(v_1,v_2)$ denotes the domain velocity obtained from solving (9a) and is therefore a known quantity for each given value of v_1 and v_2. Again, to emphasize that $n_d(E)$ depends upon both v_1 and E_m, we write $n_d(E) = n_d(E;v_1,E_m)$.

Observe that the three equations (8), (9), and (10) are coupled to each other since (8) can not be solved without first solving for $n_a(E)$ and $n_d(E)$ from (9) and (10). But (9) and (10) cannot be solved without first prescribing E_m. Consequently, we must solve (8), (9), and (10) together by an iterative method.

Notwithstanding the complexity of (6)-(10), our task for evaluating $F(v_1,v_2)$ in (6) is really a simple one conceptually since (8) is only a scalar algebraic equation and can be solved by well-known iteration techniques such as the Newton-Raphson or the Secant method [11-12] -- so long as we can devise an

algorithm for implementing this method on a computer. We will now present one such algorithm:

Algorithm for Computing $F(v_1,v_2)$, Given $(v_1,v_2) = (\bar{v}_1,\bar{v}_2)$

Step 0. Substitute $(\bar{v}_1,\bar{v}_2)$ into (8), (9), and (10).

Step 1. Assume two initial guesses $E_m^{(0)}$ and $E_m^{(1)}$.

Step 2. Let $E_m = E_m^{(k)}$ and solve the two-point boundary-value problem (9) for

$$v_D = v_D^{(k)}(\bar{v}_1,\bar{v}_2) \triangleq v_D^{(k)}, \quad k = 0,1 \tag{11a}$$

$$n_a = n_a(E;\bar{v}_1,E_m^{(k)}) \triangleq n_a^{(k)}(E), \quad k = 0,1 \tag{11b}$$

Step 3. Substitute (11a) for v_D in (10b) with k = 0 and k = 1, respectively, and solve the initial-value problem for

$$n_d = n_d(E;\bar{v}_1,E_m^{(k)}) \triangleq n_d^{(k)}(E), \quad k = 0,1 \tag{11c}$$

Step 4. Substitute (11b) and (11c) into (8) and solve for $E_m^{(k+1)}$ using the following secant iteration formula[4]

$$E_m^{(j+1)} = E_m^{(j)} - F(E_m^{(j)})\, \mathcal{G}(E_m^{(j)};\bar{v}_1,\bar{v}_2) \tag{11d}$$

where

$$F(E_m^{(j)}) \triangleq \frac{E_m^{(j)} - E_m^{(j-1)}}{\mathcal{G}(E_m^{(j)};\bar{v}_1,\bar{v}_2) - \mathcal{G}(E_m^{(j-1)};\bar{v}_1,\bar{v}_2)} \tag{11e}$$

Step 5. Iterate step 2 through 4 with the superscript "k" replaced by "j", j = 2,3,... until the iteration converges; namely,

$$n_a^{(j)}(E) \to n_a(E;\bar{v}_1,\bar{v}_2) \tag{11f}$$

$$n_d^{(j)}(E) \to n_d(E;\bar{v}_1,\bar{v}_2) \tag{11g}$$

$$E_m^{(j)} \to E_m^{(j)}(\bar{v}_1,\bar{v}_2) \tag{11h}$$

Step 6. Substitute (11f), (11g), and (11h) for $n_a(E)$, $n_d(E)$, and E_m in (6) and compute the two integrals numerically to obtain $F(\bar{v}_1,\bar{v}_2)$.

[4]For Step 4, we let k=1 and use (11d)-(11e) with "j" replaced by "k". We choose the secant method here and not the more commonly used Newton-Raphson method because the latter would require computing for the slope of $\mathcal{G}(E_m^{(j)};\bar{v}_1,\bar{v}_2)$ numerically, a rather inaccurate and time consuming task.

Observe that since $n_a(E_0) = n_a(v_1/L) = n_0$, and $n_d(E_0) = n_d(v_1/L) = n_0$, the denominators in (6), (8), (9b) and (10b) vanish at $E = E_0$. Fortunately, the corresponding numerator also vanishes at $E = E_0$ in each case. Consequently, (6)-(10) are well-defined for all $E_0 \leq E \leq E_m$ as can be verified by a straightforward application of H'opital's rule. See Appendix B for a proof of this assertion and for some techniques for avoiding numerical ill-conditioning at $E = E_0 = v_1/L$.

Since v_1 and v_2 are the two state variables associated with the circuit model in Fig. 2, and since the preceding algorithm shows how $F(v_1,v_2)$ can be computed numerically for each given value of (v_1,v_2), it follows that this circuit model can be used with any "circuit simulation program" [12] which allows the current source to be described by a special subroutine based upon the preceding algorithm. Observe that once this subroutine is included, I_D can be treated just like any other current source. In fact, we will now consider two special cases in which the subroutine for evaluating I_D can be greatly simplified.

B. Model Simplification

An examination of the circuit model of Fig. 2 shows that it already has a very simple topology and hence any further simplification should be made on the characteristics of the four circuit elements in the model. We have already shown in Footnote 2 that in so far as computer simulation is concerned, C_2 may be assigned any value since it cancells out with the corresponding C_2 in I_D and hence C_2 does not appear in the overall state equation describing the model. Consequently, we will simply set $C_2 = 1$. The nonlinear resistor R is characterized by a V_R-I_R curve identical (apart from a scaling factor) to the velocity-vs.-field characteristic $v = v(E)$. This characteristic may be represented in various forms; namely, tabular form, piecewise-linear form, or analytical form. Any simplification here will not affect the overall computational efficiency significantly. Consequently, any meaningful simplification must be made on the controlled current source I_D. Let us now consider two special cases:

Special Case 1. Constant-Diffusion Case -- $D(E) = D$

It will be shown in Section II-C that when $D(E) = D$, the domain velocity becomes identical to the electron drift velocity; namely, $v_D = v(v_1/L)$. In this case, $n_a(E)$ and $n_d(E)$ are decoupled from each other as well as from E_m, and can be computed directly from

$$f_a(n_a) = h(E;v_1) \tag{12a}$$

$$f_d(n_d) = h(E;v_1) \tag{12b}$$

where

$$h(E;v_1) \triangleq \frac{\varepsilon}{qn_0D}\int_{v_1/L}^{E}\left[v(E)-v(v_1/L)\right]\,dE \tag{12c}$$

$$f_a(n_a) = \frac{n_a}{n_0} - 1 - \ell n\,\frac{n_a}{n_0} \tag{12d}$$

$$f_d(n_d) = \frac{n_d}{n_0} - 1 - \ell n\,\frac{n_d}{n_0} \tag{12e}$$

Since $f_a'(n_a) \neq 0$ for all $n_a > n_0$ and $f_d'(n_d) \neq 0$ for all $n_d < n_0$, it follows that the inverse function $f_a^{-1}(\cdot)$ and $f_d^{-1}(\cdot)$ exist over the corresponding domain and can be computed once and for all. Hence, $n_a(E)$ and $n_d(E)$ are given explicitly by

$$n_a = n_a(E;v_1) = f_a^{-1}\Big(h(E;v_1)\Big) \tag{13a}$$

$$n_d = n_d(E;v_1) = f_d^{-1}\Big(h(E;v_1)\Big) \tag{13b}$$

Substituting (13a) and (13b) for $n_a(E)$ and $n_d(E)$ in (6) and (8) respectively, we can solve (7) for $E_m(v_1,v_2)$ directly by either the Newton-Raphson method, or the Secant method. Substituting the resulting value of E_m into (6), we can evaluate $F(v_1,v_2)$ numerically. Finally, I_D can be computed from (5) by direct substitution.

Special Case 2. Zero-Diffusion case -- $D(E) = 0$

It will be shown in Section II-C that (13a) and (13b) reduce to $n_a = \infty$ and $n_d = 0$ when $D = 0$. Under this condition, (8) can be solved explicitly for E_m; namely,

$$E_m = \frac{v_1}{L} + \sqrt{\left(\frac{2qn_0}{\varepsilon}\right)\,v_2} \tag{14a}$$

It follows from (5) and (6) that the controlled current source can be characterized explicitly by

$$I_D = C_2\int_{v_1/L}^{E_m}\left[v(v_1/L) - v(E)\right]\,dE - I \tag{14b}$$

Hence, for each given value of (v_1, v_2), we can compute for E_m explicitly from (14a). Using this value of E_m as the upper limit of integration in (14b), we can evaluate I_D by numerical integration.

C. Derivation of the Model

Consider the one-dimensional Gunn structure shown in Fig. 1(a) along with a typical carrier concentration n in Fig. 1(b), and a typical field intensity E in Fig. 1(c), at some instant of time t -- when a single high-field domain exists, or is being formed, in the region $0 < x_1 \leq x \leq x_2 < L$, henceforth referred to as the domain region. For convenience, the remaining region where $n = n_0$ and $E = E_0$ will be referred to as the "outside region". Since the diode is assumed to be one-dimensional, the current density J_1 at any point in the outside region must be equal to the current density J_2 in the domain region:

$$q\, n_0 v(E_0) + \varepsilon \frac{\partial E_0}{\partial t} = qn\, v(E) + \varepsilon \frac{\partial E}{\partial t} - q \frac{\partial}{\partial x} D(E) n \tag{15}$$

where q = electron charge, ε = dielectric constant, n_0 = electron density outside the domain, n = electron density inside the domain, E_0 = electric field outside the domain, E = electric field inside the domain; $v(\cdot)$ = electron drift velocity-vs.-field characteristic, and D(E) = field-dependent diffusion coefficient. Equation (15) can be recast into the form

$$\frac{\partial (E-E_0)}{\partial t} = \frac{qn_0}{\varepsilon} \left[v(E_0) - v(E) \right] + \frac{q}{\varepsilon} \frac{\partial D(E) n}{\partial x} - v(E) \left[\frac{q}{\varepsilon} (n - n_0) \right] \tag{16}$$

Applying Poisson's Equation $\frac{\partial E}{\partial x} = \frac{q}{\varepsilon} (n - n_0)$ to the last term in (16) and integrating both sides over the domain from x_1 to x_2, we obtain

$$\frac{dv_2}{dt} = \int_{x_1}^{x_2} \frac{qn_0}{\varepsilon} \left[v(E_0) - v(E) \right] dx + \int_{D\left(E(x_1)\right) n(x_1)}^{D\left(E(x_2)\right) n(x_2)} \frac{q}{\varepsilon}\, d\left(D(E) n\right) - \int_{E(x_1)}^{E(x_2)} v(E)\, dE \tag{17}$$

where

$$v_2 \triangleq \int_{x_1}^{x_2} (E - E_0)\, dx \tag{18}$$

is the "domain-excess" voltage. Now under our assumption of a single high-field domain with electron density n and electric field intensity E as shown

in Figs. 1(b) and (c), respectively, we see that $E(x_1) = E(x_2) = E_0$ and $n(x_1) = n(x_2) = n_0$. Hence (17) reduces to:

$$\frac{dv_2}{dt} = \int_{x_1}^{x_2} \frac{qn_0}{\varepsilon} \left[v(E_0)-v(E)\right] dx \tag{19}$$

Equation (19) is due to Kurokawa [13] and is valid regardless of the size and shape of the domain. It accurately describes the domain dynamics and is therefore valid for both transient and steady-state ($dv_2/dt=0$) analysis. Observe that in steady state (19) reduces to the well-known "equal-area rule" [1].

If we now make the additional mild assumption that the domain field E(x) has a single maximum $E = E_m$ at $x = x_3$, as in Fig. 1(c), then we can unambiguously break up the integral in (19) into two parts:

$$\frac{dv_2}{dt} = \int_{x_1}^{x_3} \frac{qn_0}{\varepsilon} \left[v(E_0)-v(E)\right] dx + \int_{x_3}^{x_2} \frac{qn_0}{\varepsilon} \left[v(E_0)-v(E)\right] dx \tag{20}$$

Applying Poisson's Equation once again to (20), we obtain

$$\boxed{\frac{dv_2}{dt} = \int_{E_0}^{E_m} \frac{n_0\left[v(E_0)-v(E)\right]}{n_a-n_0} dE + \int_{E_0}^{E_m} \frac{n_0\left[v(E_0)-v(E)\right]}{n_0-n_d} dE} \tag{21}$$

where we have replaced the symbol for electron density n by n_a in the accumulation layer ($x_1 \leq x \leq x_3$) and by n_d in the depletion layer ($x_3 \leq x \leq x_2$), in order to facilitate our subsequent interpretation. We can likewise decompose the integral in (18) into the corresponding parts from x_1 to x_3 and from x_3 to x_2, and then apply Poisson's Equation once again to obtain

$$\boxed{v_2 = \frac{\varepsilon}{q} \int_{E_0}^{E_m} \frac{(E-E_0)}{(n_a-n_0)} dE + \frac{\varepsilon}{q} \int_{E_0}^{E_m} \frac{(E-E_0)}{(n_0-n_d)} dE} \tag{22}$$

Let us next derive an expression relating the external device current I to the internal field. Since the device is one-dimensional, the total current through any cross section must be equal to the external device current. For simplicity, let us choose a cross section outside the domain so that the total current through it consists of only a carrier current component and a

displacement current component (there is no diffusion current since the field is uniform in the outside region). Hence, we have

$$\boxed{I = A\,q\,n_0 v(E_0) + \varepsilon A \frac{dE_0}{dt}} \tag{23}$$

The corresponding voltage across the device is given by

$$V = \int_0^L E(x)dx = \int_0^L E_0 dx + \int_0^L (E-E_0)dx \tag{24}$$

or

$$V = v_1 + v_2 \tag{25a}$$

where

$$v_1 = E_0 L \tag{25b}$$

can be interpreted as the voltage component due to the uniform field E_0, and where v_2 is defined earlier by (18) as that component of the domain voltage due to the electric field over and above the uniform field E_0.

Equations (21), (22), (23), and (25) completely describe the dynamics of the high-field domain in terms of the external device current I and voltage V. It remains for us to show that the equations governing the circuit model shown in Fig. 2 are given precisely by these equations. Applying first Kirchhoff current law to the upper and lower node respectively, we obtain

$$I = Aqn_0 v(v_1/L) + \left(\frac{\varepsilon A}{L}\right)\frac{dv_1}{dt} \tag{26}$$

$$I + \left[C_2 F(v_1,v_2) - I\right] = C_2 \frac{dv_2}{dt} \tag{27}$$

Simplying (27), we obtain

$$\frac{dv_2}{dt} = F(v_1,v_2) \tag{28}$$

where $F(v_1,v_2)$ is defined earlier by (6). Observe that C_2 has been cancelled in (26) and hence the state equation actually used for circuit analysis does not involve C_2 at all. Now if we substitute (25b) for v_1 in (26) and (28), we would obtain (23) and (21), respectively. Applying next Kirchhoff voltage law to the circuit model in Fig. 2, we obtain (25). Finally, let us recall that the peak-domain field E_m of our circuit model must satisfy (7) and (8).

Substituting (25b) for v_1 in (8) and using (7), we obtain (22). Hence we have proved that the governing equations of the circuit model shown in Fig. 2 are given precisely by the "physical" equations (21), (22), (23), and (25).

An examination of (21) and (22) shows that they are still incomplete in the sense that the electron density $n_a = n_a(E)$ in the accumulation layer and $n_d = n_d(E)$ in the depletion layer has not yet been specified other than that it must satisfy the following boundary conditions:

$$n(x_1) = n_a(E_0) = n_0 \tag{29a}$$

$$n(x_3) = n_a(E_m) = n_0 \tag{29b}$$

$$n(x_2) = n_d(E_0) = n_0 \tag{29c}$$

Since the high-field domain grows as it propagates from the cathode (x=0) to the anode (x=L) with an instantaneous domain velocity $v_D(t)$, the electric field intensity E and the electron density n depend upon both the "time" variable t and the "space" variable x. Hence, the <u>exact</u> form of E, n_a, and n_d must be obtained by solving the governing <u>partial</u> differential equations. It is here where some simplifying assumptions must be made in order to obviate the difficult problem of solving partial differential equations. The stronger the assumption, the easier it is to derive n_a and n_d, and of course the poorer will be the resulting approximate solution for $n_a(E)$ and $n_d(E)$.[5]

For the general field-dependent diffusion case, the external device current I can be expressed in terms of the current components inside the domain:

$$\frac{I}{Aq} = nv(E) - \frac{\partial(Dn)}{\partial x} + \frac{\varepsilon}{q}\frac{\partial E}{\partial t} \tag{30}$$

Now recall our <u>Basic Assumption (a)</u> in Section I asserts that the solution to this partial differential equation consists of a high-field domain which propagates without change of shape with the domain velocity $v_D(t)$. Consequently, if we introduce a new space variable

$$y \triangleq x - \int_0^t v_D(t)dt \tag{31a}$$

[5]Our basic assumption (a) implies that E(x) is a strictly-monotonically increasing function from $x_1 \leq x \leq x_3$, and a strictly-monotonically decreasing function from $x_3 \leq x \leq x_2$. This guarantees that n_a and n_d are well-defined <u>single-valued functions</u> of E.

and a new time variable

$$t' = t \tag{31b}$$

then (30) is transformed into the form

$$\frac{\partial(Dn)}{\partial y} = nv(E) - \frac{I}{Aq} + \frac{\varepsilon}{q}\left[-v_D \frac{\partial E}{\partial y} + \frac{\partial E}{\partial t'}\right] \tag{32}$$

Let us now invoke our Basic "Quasi-Static" Assumption (b);[6] namely

$$\frac{\partial E}{\partial t'} = 0 \tag{33}$$

Under this assumption, (23) reduces to

$$I = Aqn_0 v(v_1/L) \tag{34}$$

Substituting (33) and (34) into (32), we obtain

$$\frac{\partial(Dn)}{\partial y} = nv(E) - n_0 v(v_1/L) - \frac{\varepsilon}{q} v_D \frac{\partial E}{\partial y} \tag{35}$$

Applying Poisson's Equation, we obtain

$$\frac{\partial E}{\partial y} = \frac{\partial E}{\partial x}\frac{\partial x}{\partial y} = \frac{q}{\varepsilon}(n-n_0) \tag{36}$$

$$\frac{\partial(Dn)}{\partial y} = \frac{\partial(Dn)}{\partial E}\frac{\partial E}{\partial y} = \frac{q}{\varepsilon}(n-n_0)\left[D\frac{\partial n}{\partial E} + n\frac{\partial D}{\partial E}\right] \tag{37}$$

Substituting (36) and (37) into (35) and changing the partial differentiation operation into an ordinary differentiation operation (since the independent variable t' is no longer present), we obtain upon simplification the expression

$$\frac{dn}{dE} = \frac{n[v(E)-v_D]+n_0[v_D-v(v_1/L)]-(q/\varepsilon)(n-n_0)nD'(E)}{(q/\varepsilon)(n-n_0)D(E)} \tag{38}$$

Since (38) must hold for both n in the accumulation layer, and in the depletion layer, we obtain (9a)-(9d) by replacing n in (38) by n_a and by making use of (29a) and (29b). Similarly, we obtain (10a)-(10c) by replacing n in (38) by n_d and by making use of (29c). Observe that although (9b) and (10b) are

[6] Our Basic Assumptions (a) and (b) are similar to that made by Butcher, Fawcett, and Hilsum [14] for guaranteeing that both E and n become a function of "y" alone with the shape shown in Figs. 1(b) and (c). The new space variable "y" can be interpreted as the distance measured in a coordinate system moving in the direction of electron flow with the domain velocity $v_D(t)$.

identical in form, we have elected to solve (9) as a "two-point boundary-value" problem, thereby yielding both v_D and $n_a(E)$ as its solution. We then solve (10) as an "initial-value problem" with v_D given by (10d) representing the solution of (9). This "unsymmetrical" procedure is chosen here because solving both (9) and (10) as "two-point boundary-value" problems may not necessarily give the same value for v_D. This is because (38) is not an exact equation but is in fact derived under the two simplifying assumptions (a) and (b). In order for our solution to be consistent with assumption (a), we must force v_D to be identical in both (9) and (10) and let $n_d(E_m)$ assume whatever "slack" that may arise due to our simplifying assumptions.

The preceding material completes our derivation of the Gunn diode circuit model as described in Section II-A for the general nonlinear field-dependent diffusion case. Let us turn next to the derivation of the two simplified models described in Section II-B. Our first task will be to derive an explicit expression for the "domain velocity" v_D for the general field-dependent diffusion case by recasting (38) into the following equivalent form:

$$\left(1 - \frac{n_0}{n}\right) \frac{d\left(\frac{n}{n_0}\right)}{dE} = \frac{\varepsilon}{qn_0}\left[\frac{v(E)-v_D}{D(E)}\right] + \frac{\varepsilon}{q}\left[\frac{v_D - v(v_1/L)}{nD(E)}\right] - \frac{\left(\frac{n}{n_0} - 1\right)}{D(E)} D'(E) \tag{39}$$

Integrating both sides of (39) from E_0 to E, we obtain

$$\frac{n}{n_0} - \ell n \frac{n}{n_0} - 1 = \frac{\varepsilon}{qn_0}\int_{E_0}^{E} \frac{\left[v(E)-v_D\right]}{D(E)} dE + \frac{\varepsilon}{q}\left[v_D - v(v_1/L)\right] \int_{E_0}^{E}\left[\frac{1}{nD(E)}\right]dE$$

$$- \int_{E_0}^{E} \frac{D'(E)}{D(E)}\left[\frac{n}{n_0} - 1\right] dE \tag{40}$$

Now observe that when $E = E_m$, we have $n = n_0$ and the left-hand side of (40) vanishes. Referring to Figs. 1(b) and (c) again we see that n(x) has two branches, each of which is a single-valued function E defined over the same interval $[E_0, E_m]$. Consequently, the right side of (40) must be satisfied by both branches. If we let $E = E_m$ in (40) and pick the left branch corresponding to the accumulation layer with $n = n_a$, we would obtain

$$0 = \frac{\varepsilon}{qn_0}\int_{E_0}^{E_m} \frac{\left[v(E)-v_D\right]}{D(E)} dE + \frac{\varepsilon}{q}\left[v_D - v(v_1/L)\right] \int_{E_0}^{E_m} \frac{1}{n_a D(E)} dE - \int_{E_0}^{E_m} \frac{D'(E)}{D(E)}\left[\frac{n_a}{n_0} - 1\right] dE \tag{41}$$

Similarly, if we pick the right branch corresponding to the depletion layer with $n = n_d$, we would obtain

$$0 = \frac{\varepsilon}{qn_0}\int_{E_0}^{E_m}\frac{[v(E)-v_D]}{D(E)}\,dE + \frac{\varepsilon}{q}\left[v_D - v(v_1/L)\right]\int_{E_0}^{E_m}\frac{1}{n_d D(E)}\,dE - \int_{E_0}^{E_m}\frac{D'(E)}{D(E)}\left[\frac{n_d}{n_0}-1\right]dE \tag{42}$$

Subtracting (42) from (41) and solving for v_D, we obtain [9].

$$v_D = v(v_1/L) - \frac{q}{\varepsilon}\left\{\frac{\displaystyle\int_{v_1/L}^{E_m}\frac{D'(E)}{n_0 D(E)}\left[n_a(E)-n_d\right]dE}{\displaystyle\int_{v_1/L}^{E_m}\frac{1}{D(E)}\left[\frac{1}{n_d(E)}-\frac{1}{n_a(E)}\right]dE}\right\} \triangleq v_D(v_1,v_2) \tag{43}$$

Observe that (43) can be computed only after E_m, $n_a(E)$, and $n_d(E)$ have been found using either the algorithm given in Section II-A, or other approximation techniques. Observe also that v_D is shown as a function of v_1 and v_2 since v_1 is present explicitly in (43) and since E_m depends implicitly on both v_1 and v_2. We are now ready to consider the two special cases in Section II-B:

Special Case 1. Constant-Diffusion Case -- $D(E) = D$.

Substituting $D'(E) = 0$ in (43), we obtain

$$v_D = v(v_1/L) \tag{44}$$

Hence, in the constant-confusion case, the domain velocity is equal to the electron-drift velocity [14]. Substituting (44) for v_D in (40) and then letting $n = n_a$ and $n = n_d$ respectively, we obtain

$$\frac{n_a}{n_0} - \ell n\frac{n_a}{n_0} - 1 = \frac{\varepsilon}{qn_0 D}\int_{v_1/L}^{E}\left[v(E)-v(v_1/L)\right]dE = h(E;v_1) \tag{45a}$$

$$\frac{n_d}{n_0} - \ell n\frac{n_d}{n_0} - 1 = \frac{\varepsilon}{qn_0 D}\int_{v_1/L}^{E}\left[v(E)-v(v_1/L)\right]dE = h(E;v_1) \tag{45b}$$

where $h(E;v_1)$ is defined earlier in (12c). Substituting (12d) and (12e) into (45a) and (45b), we obtain (12a) and (12b) which in turn lead to (13a) and (13b).

Special Case 2. Zero-Diffusion Case -- $D(E) = 0$.

Observe that the right-hand size of both (45a) and (45b) tends to ∞ as we let D tend to zero. This implies that $n_a \to \infty$ and $n_d \to 0$ because

$$\lim_{n_a \to \infty} \left\{ \frac{n_a}{n_0} - \ell n \frac{n_a}{n_0} - 1 \right\} = \lim_{n_a \to \infty} \frac{n_a}{n_0} \left\{ 1 - \frac{\ell n \frac{n_a}{n_0}}{\frac{n_a}{n_0}} - \frac{1}{\frac{n_a}{n_0}} \right\} = \infty \tag{46a}$$

and

$$\lim_{n_d \to 0} \left\{ \frac{n_d}{n_0} - \ell n \frac{n_d}{n_0} - 1 \right\} = \lim_{n_d \to 0} \left\{ \frac{n_d}{n_0} + \ell n \frac{n_0}{n_d} - 1 \right\} = \infty \tag{46b}$$

Substituting $n_a = \infty$ and $n_d = 0$ into (22), we obtain

$$v_2 = \frac{\varepsilon}{q n_0} \int_{v_1/L}^{E_m} [E - v_1/L] dE \tag{47}$$

Integrating (47) directly and solving for E_m, we obtain (14). Similarly, substituting $n_a = \infty$ and $n_d = 0$ into (6), we obtain

$$F(v_1, v_2) = \int_{v_1/L}^{E_m} \left[v(v_1/L) - v(E) \right] dE \tag{48}$$

Finally, substituting (48) into (5), we obtain (15).

D. Comparison with Other Models

Comparing our circuit model in Fig. 2 with Robrock's model [6] for the single-domain case, we find that they are idenctical in both topology and the type of circuit elements. However, there are also significant differences. For example, the domain capacitance C_2 in our model is linear whereas that in Robrock's model is nonlinear. The most important difference, however, is in the characterization of the controlled current source I_D. In our model, I_D may assume many different forms depending upon the simplifying assumptions made in reducing the exact partial differential equations into approximate ordinary differential equations. The characterization given in our paper along with the two special cases represent only three reasonable choices. It is conceivable that other equally reasonable or better assumptions may be found which give rise to other characterizations. In contrast to this, the current

source I_D in Robrock's model is given by a purely empirical curve depending only on the domain voltage v_2. Since I_D must depend also on the terminal current I in order for Robrock's circuit model to be consistent with the governing physical equations, the violation of a "current-conservation law" in Robrock's model as pointed out by Gunshor and Kak [7] can be traced to the characterization of I_D.

Comparing next our circuit model with the Gunshor-Kak model [7-8], we note first that one has 4 circuit elements, the other has 5, two of them are controlled sources -- a linear voltage-controlled voltage source V_{ex} and a nonlinear voltage-controlled current source $I_{DD}(E_0,E_D)$. However, it is interesting to observe that inspite of the differences in the network topology and the number of circuit elements between these two models, it can be easily verified that the governing equations derived from these two models are identical in the zero-diffusion case: In other words, so long as the domain has not yet reach the anode, then both circuit models would yield identical answers, when imbedded in the same external circuit, provided $D(E) = 0$. These two models differ drastically, however, in the nonzero-diffusion case. Here the nonzero-diffusion effect is treated only very briefly in an ad hoc manner in [7] whereas an arbitrary nonlinear diffusion characteristic D(E) is allowed in our model. Observe also that the parameter I_{DD} in the Gunshor-Kak model depends on two space variables x_1 and x_2 whereas all parameters in our model are circuit variables.

III. COMPLETE LUMPED CIRCUIT MODEL INCLUDING DOMAIN EXTINCTION (AT THE ANODE) AND NUCLEATION PHENOMENA

The circuit model shown in Fig. 2 is valid so long as the domain is extinguished by the external circuit constraints before it gets to the anode, such as in the quenched-domain mode, or when a "mature" domain does not exist, such as in the LSA mode. However, in the transit-time mode, or in the delayed-domain mode, this model is valid only during the time interval where the domain is in motion and has not yet reached the anode. In order to model the domain extinction phenomena at the anode, it suffices to devise a timing circuit which "tracks" the domain motion and causes the domain capacitor C_2 to discharge quickly whenever the domain reaches the anode. This timing circuit is then added to the circuit of Fig. 2 to obtain the complete circuit model shown in Fig. 3. The nonlinear controlled current source is given by

$$I_C = Aqn_0\, v_D(v_1, v_2) \tag{49}$$

in the general case where $D'(E) \neq 0$. However, in the constant-diffusion case, we can obtain from (44) the relationship $v_D = v(v_1/L)$ and then using (4), we can simplify (49) to obtain:

$$I_C = Aqn_0\, v(v_1/L) = I_R \tag{50}$$

Hence, in the constant-diffusion case, the nonlinear controlled source I_C reduces to a linear controlled current source depending only on the current I_R of the nonlinear resistor R. The three voltage-controlled nonlinear resistors behave like "relays" which are activated whenever a prescribed threshold voltage is reached; namely,

$$R_1(v_1) = \begin{cases} 0, & v_1 \geq E_t L \triangleq v_{1t} \\ \infty, & v_1 < E_t L \triangleq v_{1t} \end{cases} \tag{51}$$

where E_t is the "threshold" field intensity when the drift velocity curve $v(E)$ attains its maximum.

$$R_2(v_2) = \begin{cases} 0, & v_2 = 0 \\ \infty, & v_2 \neq 0 \end{cases} \tag{52}$$

$$R_3(v_3) = \begin{cases} \tau_d/C_2, & v_3 \geq Aqn_0 L \triangleq v_{3t} \\ \infty, & v_3 < Aqn_0 L \triangleq v_{3t} \end{cases} \tag{53}$$

where C_2 is the domain capacitance (usually set equal to unity for convenience) and τ_d is a very small number chosen equal to the "average" time constant for the domain to collapse (τ_d is of the order of a few hundred picoseconds [2]). From the computer simulation point of view, a separate subroutine for implementing (51), (52), and (53) via efficient logic statements should be used. This is because the augmented timing circuit shown in Fig. 3 comes into play only momentarily whenever a high-field domain reaches the anode. It does not affect the domain dynamics at all and therefore should be included in the computation only when needed. Hence, considerable computer time can be saved if a special subroutine is used in place of the timing circuit. Also observe that the circuit model in Fig. 2 is much more efficient computationally when $D(E) = 0$ and should therefore be used in most computer simulation analysis

when the error due to this assumption is tolerable. The complete Gunn diode circuit model for the zero-diffusion case is redrawn in Fig. 4 to emphasize the simplifications resulting from assuming D(E) = 0. Among other things, we note the controlled current source I_C in the timing circuit now depends directly on the current I_R of the nonlinear resistor. But the most dramatic simplification is in I_D where it can now be evaluated explicitly by using (14) and (15) without having to solve any algebraic or differential equations. The dotted lines in Fig. 4 are included to help locate where the controlling variables are.

To understand the operation of the timing circuit, observe first that the two resistors R_1 and R_2 are always open whenever $v_1 < v_{1t}$ and $v_2 \neq 0$. Physically, this means that whenever the domain is being formed and transported towards the anode, the current source I_C flows directly into the timing capacitor C_3 and charges it until v_3 reaches the threshold value $v_3 = v_{3t}$. At this point R_3 changes from an open circuit to a very small resistance, thereby allowing the domain capacitance voltage v_2 to discharge rapidly. It remains for us to show that the total time T_D it takes the current source I_C to charge the capacitor C_3 from $v_3 = 0$ to $v_3 = v_{3t}$ is precisely equal to the time it takes the domain to traverse from the cathode at x = 0 to the anode at x = L. To show this, observe that whenever $v_1 < v_{1t}$ and $v_2 \neq 0$, both $R_1(v_1) = \infty$ and $R_2(v_2) = \infty$ and hence we have $v_3(t) = \int_0^t Aqn_0\, v_D(\tau)d\tau$. Substituting $v_3(t) = v_{3t} = Aqn_0L$ at $t = T_D$ into this expression and simplifying, we obtain

$$L = \int_0^{T_D} v_D(\tau)d\tau \tag{54}$$

This relation verifies that the domain indeed reaches the anode (x=L) at precisely $t = T_D$. Observe that T_D depends on the external circuit in general since the domain velocity $v_D(t)$ depends on both v_1 and v_2.

In the transit-time mode where the terminal voltage is constrained by a dc or ac bias voltage source with amplitude $V_B > v_{1t}$, the voltage v_1 must increase as the domain voltage v_2 collapses in order to take up the slack. Consequently, v_1 will reach v_{1t} before v_2 goes to zero, thereby activating R_1. Hence in the transit-time mode $v_2 \neq 0$ and R_2 remains an open circuit at all times. On the other hand, in the quenched-domain mode where the domain never

reaches the anode, or in the LSA mode where a "mature" domain does not exist, we have $v_3 < v_{3t}$ and hence the timing circuit is automatically deactivated at all times even though R_2 may switch on and off periodically. Observe also that if the dc bias voltage is smaller than v_{1t} and if $v_2(t) = 0$, then no domain will form and hence $v_2(t) = 0$ for $t \geq 0$. In this case we have $R_1 = \infty$, $R_2 = 0$, and the timing circuit is once again deactivated at all times. In other words, the timing circuit comes into play in the sense that R_3 changes state periodically only in the transit-time mode and in the delayed-domain mode. The controlled resistors R_1 and R_2 are used to reset the capacitor voltage v_3 to zero in the transit-time mode and in the delayed-domain mode, respectively, whenever the domain begins to build up at the cathode, thereby allowing C_3 to keep track with the domain motion. Notice that our preceding analysis allows the domain velocity v_D to vary with time. Consequently, given any external circuit, our timing circuit can indeed precisely predict the time when a domain reaches the anode.

Observe also that as soon as the capacitor voltage v_3 has been reset to zero, we have $R_3 = \infty$ and a domain will be nucleated thereafter whenever $v_1 \geq v_{1t}$. In the transit-time mode, this starting condition occurs at the same time when v_3 changes to zero because v_1 must have increased to v_{1t} in order to take up the slack due to the bias voltage. However, in the remaining modes, the domain-starting condition will depend on the amplitude of the waveform across the diode. In any event, our timing circuit will allow a domain to nucleate at the appropriate point in time.

In actual implementation of this model for computer simulation, we have found it desirable to replace (53) by a continuous function such as

$$R_3(v_3) \triangleq \frac{\tau_{d0}}{C_2} \left\{ e^{500[1-v_3/Aqn_0L]} \right\} \tag{55}$$

where τ_{d0} is some appropriately chosen time constant. Finally, observe that since $dv_2/dt = 0$ whenever $v_2 = 0$, it is necessary to insert a small "noise" current source in parallel with the domain capacitance in any computer simulation in order that a domain may be nucleated automatically even when $v_2 = 0$.

IV. COMPUTER-SIMULATED EXAMPLES

Our objective in this section is to present a number of examples for demonstrating the validity of our circuit model under any loading condition

when the diode is connected across an arbitrary external circuit. In particular, we will show that for the same set of model parameters associated with a given Gunn diode,[7] our model can indeed predict, among other things, the four well-known Gunn diode steady-state operating modes [3]; namely, the transit-time mode, the delayed-domain mode, quenched-domain mode, and the LSA mode. We will also show that our model is suitable for simulating transient behaviors such as those associated with Gunn logic circuits [2].

Five examples will be presented in this section. Since the "zero-diffusion" model shown in Fig. 4 is much more efficient computationally, these examples will be simulated on the computer using this model in order to emphasize that the "zero-diffusion" model is adequate for most purposes. Our first four examples are concerned with simulating the steady-state waveforms associated with the "single-cavity" Gunn-diode circuit shown in Fig. 5(a), where the cavity is modelled by a parallel resonant circuit. The relevant model parameters and the associated nonlinear resistor V_R-I_R curve chosen for this example are also specified in Fig. 5(a). The external circuit parameters R, L, C, and V_B for the first four examples are tabulated as shown in Fig. 5(b). The waveforms to be simulated in each example consists of the following:

a) Steady-state waveform for diode terminal voltage V(t).

b) Steady-state waveform for diode terminal current I(t).

c) Steady-state waveform for the "excess" capacitor voltage $v_1(t)$ across capacitor C_1. (Recall that $v_1(t) = E_0(t)L$, where $E_0(t)$ is the excess electric field intensity at time t, and L is the device length.

d) Steady-state waveform for the "domain" capacitor voltage $v_2(t)$ across capacitor C_2.

e) Steady-state waveform for the "timing" capacitor voltage $v_3(t)$ across capacitor C_3.

---

[7] While a model can only be an approximation of a device [12], it must at least have the ability to predict correctly the qualitative behavior of the device when imbedded in an arbitrary external circuit. This implies that given a device, its associated model parameters can be determined once and for all through a combined experimental and numerical method. Once the model parameters are found, the circuit model is completely specified and can be used for simulating an arbitrary circuit containing the device.

[8] We have abused our notation slightly by using L to denote both the device length and the inductance of the resonant circuit. However, the context will make it clear which meaning to assign.

For purposes of comparison among different devices, the waveform associated with the following normalized variables will be plotted:

Normalized Voltages	Normalized Current
$\bar{V} \triangleq V/E_tL$, $\bar{v}_1 \triangleq v_1/E_tL$, $\bar{v}_2 \triangleq v_2/E_tL$	$\bar{I} \triangleq I/Aqn_0\mu E_t$

where E_t denotes the threshold electric field of the velocity-vs.-field curve, and μ denotes the mobility of the electrons. For our first four examples, we have $V_t \triangleq E_tL = 4$ volts and $I_t \triangleq Aqn_0\mu E_t = 0.512$ mA.

Example 1. Transit-Time Mode

Using the model and circuit parameters given in Fig. 5 for the transit-time mode, the normalized steady-state voltage waveforms $\bar{V}(t)$, $\bar{v}_1(t)$, $\bar{v}_2(t)$, and the unnormalized voltage $v_3(t)$ are shown in Figs. 6(a), (b), (c), and (d), respectively. The normalized steady-state current waveform $\bar{I}(t)$ is shown in Fig. 7(b), where the associated $\bar{V}(t)$ is repeated in Fig. 7(a) for comparison purposes. The "ac" $\bar{I}$-$\bar{V}$ curve obtained by plotting the Lissajous figure corresponding to $\bar{I}(t)$ and $\bar{V}(t)$ is shown by the loop labelled ①, ②, ③, ④ in Fig. 7(c).

The operation of the transit-time mode can be illustrated with the help of Fig. 6. First we recall that the sawtooth-like waveform $v_3(t)$ in Fig. 6(d) serves as a time base whose period is automatically set equal to the total time it takes a high-field domain to traverse from the cathode to the anode with a not-necessarily constant domain velocity v_D. Let us examine the sequence of events over one period starting at point ① which corresponds to the time when the domain reaches the anode. Referring to (52), this occurs when $v_3(t)$ increases to Aqn_0L, at which point, resistor R_3 switches to τ_d/C_2, where τ_d is of the order of a few hundred picoseconds [2]. Hence the domain capacitor voltage $\bar{v}_2$ discharges rapidly through R_3 with a time constant equal to τ_d.[9] An examination of Figs. 6(a), (b), and (c) shows that as $\bar{v}_2(t)$ drops, $\bar{v}_1(t)$ increases in order to take up the slack until $v_1(t) \triangleq (E_tL)\bar{v}_1(t) = E_tL$, i.e., until $\bar{v}_1(t) = 1$ (point ②). At this point in time, $R_1(v_1)$ switches momentarily from an open to a short circuit and $v_3(t)$ drops instantaneously to zero (also labelled ②). This effectively forces $R_1(v_1)$ to switch immediately back to

[9] To avoid dealing with discontinuous functions, our examples in this section are all simulated with a continuous $R_3(v_3)$ as given by (54), which results in an approximately equal time constant for the discharge waveform.

an open circuit and the capacitor C_3 begins to charge through the "time-base" current source I_C. Observe that point (2) at $v_3(t) = 0$ corresponds to the nucleation of a new domain at the cathode. As the domain voltage $\bar{v}_2(t)$ increases, $\bar{v}_1(t)$ decreases as shown in Figs. 6(c) and (b), respectively. Point (3) is located where the high-field domain has matured into a steady state and subsequently, $\bar{v}_1(t)$ and $\bar{v}_2(t)$ must remain constant as the domain traverses toward the anode. Observe that since $\bar{v}_2(t) > 0$ for all times in Fig. 6(c), the resistor $R_2(v_2)$ in the transit-time mode is always an open circuit. Finally, as the "time-base" voltage $v_3(t)$ reaches point (4) corresponding to the time instant where the domain arrives at the anode, the cycle repeats itself.

The portion of the $\bar{I}$-$\bar{V}$ curve shown in Fig. 7(c) from point (1) to point (4) is the Lissijous figure associated with the steady-state waveforms shown in Figs. 7(a) and (b) and will henceforth be referred to as the "ac" $\bar{I}$-$\bar{V}$ curve. Observe that the dotted portion corresponds to the time interval where the domain is either being discharged, or being formed. The small solid segment between points (3) and (4) corresponds to the time interval where the domain has matured to a steady state and is traversing toward the anode. The overall curve formed by the dash lines and the short solid line segment is the "dc" $\bar{I}$-$\bar{V}$ curve to be described in the next section.

Example 2. Delayed-Domain Mode

Using the model and circuit parameters given in Fig. 5 for the delayed-domain mode, the normalized steady-state voltage waveforms $\bar{V}(t)$, $\bar{v}_1(t)$, $\bar{v}_2(t)$, and the unnormalized voltage $v_3(t)$ are shown in Figs. 8(a), (b), (c), and (d), respectively. The normalized steady-state current waveform $\bar{I}(t)$ is shown in Fig. (9) (b), where the associated $\bar{V}(t)$ is repeated in Fig. 9(a) for comparison purposes. The "ac" $\bar{I}$-$\bar{V}$ curve obtained from Figs. 9(a) and (b) is shown by the solid and dotted portion of the curve in Fig. 9(c).

The operation of the delayed-domain mode can be illustrated with the help of Fig. 8. Again, let us begin at point (1) on the time-base voltage waveform $v_3(t)$ corresponding to the time instant when the domain reaches the anode, thereby switching $R_3(v_3)$ to its low-resistance state. Hence, the domain capacitor voltage $\bar{v}_2(t)$ discharges rapidly through R_3 until it reaches zero volt (point (3)) at which time resistor $R_2(v_2)$ switches from an open to a short circuit. From here on the domain remains extinguished while $\bar{v}_1(t)$ takes up whatever slack needed to satisfy KVL in order to maintain a nearly

sinusoidal voltage $\bar{V}$ across the high-Q resonant circuit. As $\bar{v}_1(t)$ increases beyond the threshold votlage $\bar{v}_1 = 1$ (point ⑤), $R_1(v_1)$ switches from a short to an open circuit. A slight increment of time thereafter, $\bar{v}_2$ becomes positive once again since $\bar{V}$ continues to increase at point ⑤. This causes $R_2(v_2)$ to switch from a short to an open circuit, thereby starting the time-base sawtooth waveform until the domain reaches the anode, and then the cycle repeats itself.

The "ac" $\bar{I}$-$\bar{V}$ curve corresponding to the waveforms in Figs. 9(a) and (b) is shown in Fig. 9(c) to consist of 2 dotted segments and 2 solid segments. The dotted segments correspond to the interval where the domain is in motion; i.e., either growing or decaying. The solid segments correspond to the intervals where the "mature" domain is in transit between points ⑥ and ⑦, or when the domain is in its extinguished state between points ③ and ⑤. The overall curve made up by the dash and solid segments constitute the "dc" $\bar{I}$-$\bar{V}$ curve whose significance is to be presented in the next section.

Finally, we remark that the origin of the name "delayed-domain" mode comes from the observation that a new domain is not formed until the excess capacitor voltage $v_1(t)$ rises above its threshold value. The delay in the initiation of a new domain is due to the near-sinusoidal nature of $\bar{V}(t)$ which prevents $v_1(t)$ from assuming a higher voltage before point ⑤.

Example 3. Quenched-Domain Mode

Using the model and circuit parameters given in Fig. 5 for the quenched-domain mode, the normalized steady-state voltage waveforms $\bar{V}(t)$, $\bar{v}_1(t)$, $\bar{v}_2(t)$, and the unnormalized voltage $v_3(t)$ are shown in Figs. 10(a), (b), (c), and (d), respectively. The normalized steady-state current waveform $\bar{I}(t)$ is shown in Fig. 11(b), where the associated $\bar{V}(t)$ is repeated in Fig. 11(a) for comparison purposes. The "ac" $\bar{I}$-$\bar{V}$ curve obtained from Figs. 11(a) and (b) is shown by the solid and dotted portion of the curve in Fig. 11(c).

The operation of the quenched-domain mode can be illustrated with the help of Fig. 10. Unlike the preceding examples, let us start with point ① in Fig. 10(c) where the domain voltage $v_2(t)$ drops to zero, thereby switching $R_2(v_2)$ to a short circuit. This causes $v_3(t)$ to drop instantaneously to zero and remain so until $\bar{v}_1(t)$ rises above the normalized threshold voltage $\bar{v}_1 = 1$ at point ④, thereby switching $R_1(v_1)$ to an open circuit. Thereafter the domain voltage $\bar{v}_2(t)$ begins to build up while the time-based voltage $v_3(t)$

rises to keep track of its motion. In sharp contrast with the operation of the preceding examples, however, observe that the domain voltage $\bar{v}_2(t)$ becomes zero at point (1) before the domain reaches the anode. Consequently, $R_3(v_3)$ remains an open circuit for all times and the timing circuit therefore plays no role in determining the waveforms in the quenched-domain mode. The term "quench" is used to emphasize that the high-field domain in this case is extinguished by the waveform $\bar{V}(t)$, and not by discharging at the anode.

The "ac" $\bar{I}$-$\bar{V}$ curve associated with the waveforms in Figs. 11(a) and (b) is given by the dotted and solid portion of Fig. 11(c). The dotted portion corresponds to the intervals where the domain is being formed, or being quenched, while the solid portions correspond to the intervals where the domain has reached a steady state. As before, the overall curve consisting of the dash lines and the solid portion is the "dc" $\bar{I}$-$\bar{V}$ curve.

Example 4. LSA Mode

The waveforms corresponding to the preceding examples for the LSA mode are shown in Figs. 12 and 13. Here, we observe that $\bar{v}_1(t) \cong \bar{V}(t)$ because $\bar{v}_2(t) = 0$ everywhere except over a very small time interval where $\bar{v}_2(t)$ increases to no larger than 0.01. Consequently, $R_2(v_2)$ becomes a short circuit most of the time, and the domain can be assumed to be almost non-existing. Since the time-base voltage $v_3(t)$ is also almost zero, $R_3(v_3)$ remains an open circuit for all time in the LSA mode.

The "ac" $\bar{I}$-$\bar{V}$ curve associated with the waveforms in Figs. 13(a) and (b) is given by the dotted curve in Fig. 13(c).

Our fifth and final example is concerned with simulating the transient waveforms using the zero-diffusion circuit model shown in Fig. 4.

Example 5. Gunn-Diode Logic AND Gate

Consider the two-Gunn-diode logic circuit shown in Fig. 14(a) along with a truth table taken from [2] which describes the basic logic operation due to two input voltage waveforms $v_{S1}(t)$ and $v_{S2}(t)$. Observe that only when both inputs assume positive values do we get a positive output voltage -- hence the name AND gate. For this example, we choose the two "unsymmetrical" square-waves shown in Fig.s 14(b) and (c) as the inputs. The resulting output voltage $v_0(t)$ as simulated by the computer using our zero-diffusion circuit model is shown in Fig. 14(d). A comparison of the three waveforms $v_{S1}(t)$, $v_{S2}(t)$, and

$v_0(t)$ shows that the circuit does behave in accordance with the logic operation tabulated in Fig. 14(a).

V. DC I-V CURVE OF GUNN DIODE AND ITS INTERPRETATION

An examination of the "ac" $\bar{I}$-$\bar{V}$ curve associated with the normalized terminal voltage $\bar{V}(t)$ and current $\bar{I}(t)$ of the Gunn diode in Figs. 7(c) , 9(c), 11(c) and 13(c) reveals that the solid portion of each "ac" $\bar{I}$-$\bar{V}$ curve lies on an identical curve. From our past experience with oscillator circuits containing locally active 2-terminal elements -- such as tunnel diodes -- it is indeed tempting to define a "dc" I-V curve for the Gunn diode shown in Fig. 5(a) and then use it to explain and predict circuit behaviors. Our objective in this final section is to show how this can be done in a meaningful and rigorous way.

Since the solid portions of the "ac" $\bar{I}$-$\bar{V}$ curves in the preceding section are all associated only with the "domain model" shown in Fig. 2, and since the dotted portions of these curves are clearly time-varying in nature, any reasonable definition of a "dc" I-V curve must be associated with the domain model. From the circuit and system-theoretic point of view, this circuit model can be considered as a dynamic nonlinear one-port characterized by a "state" equation and an "output" equation as follow [12,15]:

State Equation:

$$\frac{dv_1}{dt} = \frac{1}{C_1}\left[I - G(v_1)\right] \tag{56a}$$

$$\frac{dv_2}{dt} = F(v_1, v_2) \tag{56b}$$

Output Equation:

$$V = v_1 + v_2 \tag{56c}$$

where $G(v_1)$ and $F(v_1,v_2)$ are defined by (4) and (6), respectively. Equation (56) completely characterizes the circuit model of Fig. 2 in the sense that given any external circuit connected to the Gunn diode, one could simulate the solutions using the above equation in place of the circuit model. Observe that for each given value of I, (56a) and (56b) represent a system of two autonomous

equations [16-17] whose equilibrium states are simply obtained by equating (56a) and (56b) to zero and then solving for (v_1,v_2). Hence, we can obtain a relation between the "dc" port current I and the associated port voltage V in equilibrium by eliminating the two variables v_1 and v_2 from the following three equilibrium equations derived from (56):

$$I - G(v_1) = 0 \tag{57a}$$

$$F(v_1,v_2) = 0 \tag{57b}$$

$$V - v_1 - v_2 = 0 \tag{57c}$$

The solutions of (57) represent a set $\mathcal{S}$ of points in the I-V plane and it is this set $\mathcal{S}$ that we will define as the "dc" I-V curve of the Gunn diode. The set $\mathcal{S}$ can be obtained by solving (57) numerically, or graphically. For the zero-diffusion case, $F(v_1,v_2)$ is given simply by (48), where E_m is given by (14). The resulting curve is shown in Fig. 15(a) in terms of the normalized variable $\bar{V}$ and $\bar{I}$ defined earlier. Observe that this "dc" $\bar{I}$-$\bar{V}$ curve is a multivalued function of both terminal variables $\bar{I}$ and $\bar{V}$. A comparison between this curve and those of Figs. 7(c), 9(c), 11(c), and 13(c) shows that the solid portions of the latter are identical to the former. In other words, we have just verified that the solid portions of the "ac" $\bar{I}$-$\bar{V}$ curves actually lie on the "dc" $\bar{I}$-$\bar{V}$ curve. We also observe that the two points "T" (for threshold) and "Q" (for quenched) on the "dc" $\bar{I}$-$\bar{V}$ curve are of special interest because each is connected to the solid portion of the "ac" $\bar{I}$-$\bar{V}$ curve by dotted lines representing the domain transient buildup and decay. The obvious question to raise at this point is why doesn't any point on the "ac" $\bar{I}$-$\bar{V}$ curves in Figs. 7(c), 9(c), 11(c), and 13(c) fall on the segment of the "dc" $\bar{I}$-$\bar{V}$ curve between points T and Q?

The answer to the above question becomes obvious if we recall that each point (V_p,I_p) on the $\bar{I}$-$\bar{V}$ curve $\mathcal{S}$ corresponds to an equilibrium point of the autonomous system (56a)-(56b) with $I = I_p$. Since an equilibrium point may be either locally attracting (stable) or repelling (unstable) [16-17], it follows that each point P on the "dc" $\bar{I}$-$\bar{V}$ curve can be either "attacting" or "repelling" in a neighborhood of P. The stability or instability of each equilibrium point can be determined by examining whether the eigen-value of the associated Jacobian matrix evaluated at P lies in the left- or in the right-half plane.

Such an analysis has in fact been carried out for all points along the dc $\bar{I}$-$\bar{V}$ curve and the result (for any v(E)-vs.-E curve passing through the origin with a positive slope and having a single maxima and minima) can be summarized as follow:

Region	Type of Equilibrium Point	Property
From $-\infty$ to T	Node	Stable
From T to Q	Saddle point	Unstable
From Q to $+\infty$	Node	Stable

It is interesting to observe that our analytical result here agrees with the computer-simulated results obtained by Kak and Gunshor [8]. In particular, our region from T to Q corresponds to their $|gR_0| > 1$ region, and our region from Q to $+\infty$ corresponds to their $|gR_0| < 1$ region. In fact, it can be shown analytically that our "quenching point" Q corresponds precisely to their critical condition $gR_0 = 1$. Figure 15(b) shows a typical "dc" $\bar{I}$-$\bar{V}$ curve with the type and stability of each corresponding equilibrium point indicated on the curve. Now it is clear why the "ac" $\bar{I}$-$\bar{V}$ curve cannot fall on the segment between T and Q if the input current I is held constant. For our examples, $\bar{I} = \bar{I}(t)$ is a time-varying waveform and the above conclusion is no longer valid in general. Howeve, if $\bar{I}(t)$ changes much more slowly than the settling time associated with (56), then $\bar{I}(t)$ can be considered as a constant in a small neighborhood of any time t and the same conclusion holds. An examination of the time scales involved in the waveforms given in Figs. 8-11 shows that this is indeed the case because the domain "build up time" is only a small fraction of the period of the associated waveforms.

From the physical point of view, the above conclusion can also be derived by observing that after a domain matures and propagates toward the anode, the "excess" uniform field E_0 no longer depends on the domain dynamics, but only on the external waveform $\bar{V}(t)$ in order to satisfy KVL. In other words, $v_1(t) = E_0(t)L$ serves only as a "slack variable" independent of the domain dynamics. Hence both the excess capacitor C_1 and the domain capacitor C_2 can be replaced by open circuits as soon as the domain has grown to maturity The resulting circuit is purely resistive and is in fact characterized by the same "dc" $\bar{I}$-$\bar{V}$ curve defined earlier.

The above interpretation of the significance of the "dc" I-V curve clearly shows that it can be used meaningfully just like a nonlinear resistor -- such as tunnel diode -- over any time interval where a matured-domain is propagating towards the anode.

VI. CONCLUDING REMARKS

We have demonstrated through examples that the zero-diffusion circuit model is capable of predicting correctly the qualitative behaviors and waveforms associated with Gunn-diode circuits. Since the zero-diffusion model is computationally much more efficient, it should be chosen first in any computer simulation analysis. Only when there is reason to believe that the answers to a particular circuit will depend strongly on a nonlinear diffusion characteristic $D = D(E)$ should the general circuit model given in Section II-A be chosen.

We have given a rigorous definition of a "dc" I-V curve for Gunn diodes and have shown that so long as the circuit is operating while a matured domain is traversing towards the anode, the circuit can be correctly analyzed by replacing the Gunn diode by a nonlinear resistor characterized by this "dc" I-V curve. Since circuit engineers are much more familiar with the analysis of tunnel diode circuits, and since the "dc" I-V curve for Gunn diodes resembles that of a tunnel diode, this observation should come in handy in the analysis and design of Gunn-diode circuits.

Finally, we remark that although the $\bar{I}$-$\bar{V}$ curve shown in Fig. 13(c) for the LSA mode is a continuous and single-valued function, it is nevertheless an "ac" I-V curve valid only over the frequency range for LSA operation. Observe that the solid portion on this curve falls on the "dc" $\bar{I}$-$\bar{V}$ curve because the domain does not exist in the region $\bar{V} < 1$ for all frequencies, including dc. Beyond $\bar{V} = 1$, a matured-domain would generally exist unless the operating frequency is so high that the domain has no time to build up, which is exactly the condition for the LSA mode. Under this situation, the capacitor C_2 becomes almost a short circuit and we have $V(t) \approx V_R(t) \approx v_1(t)$. Moreover, the value of C_1 is typically so small that the current $i_{c_1}(t)$ through C_1 in the LSA mode is negligible compared to $I_R(T)$. Hence, we expect the "ac" $\bar{I}$-$\bar{V}$ curve associated with the LSA mode to be simply the I_R-vs.-V_R curve of the nonlinear resistor R. This is precisely what we obtained in Fig. 13(c).

APPENDIX

A. THE MODIFIED SHOOTING METHOD

The "shooting-method" often refers to a well-known technique for transforming a boundary-value problem into an initial-value problem by finding an appropriate initial condition which forces the resulting solution to satisfy the prescribed boundary condition [11]. Our problem of finding an appropriate domain velocity v_D in solving (9a) subject to the two boundary conditions (9c) and (9d) is quite different from the above initial-value problem. However, it can be solved by a method analogous to that of the shooting method.

The basic idea behind our "modified" shooting method can be explained with the help of Fig. 16(a) where the solution to the initial-value problem 9(a) subject to the single initial condition (9c) is shown for three different values of v_D. Observe that only the solution corresponding to $v_D = v_D^*$ will satisfy the boundary condition (9d) and is therefore the desired solution. Our problem is to find v_D^*. A typical solution $n_a = n_a(E)$ for $v_D \neq v_D^*$ is shown if Fig. 16(b). Notice that $n_a = n_0$ at $E = E_0$ and at $E = E_p(v_D)$, where $E_p(v_D) \neq E_m$. If we define $\mathcal{E}(v_D) = E_m - E_p(v_D)$, then our objective is to find v_D such that the "error" $\mathcal{E}(v_D) = 0$. This is analogous to finding an appropriate velocity such that a projectile starting form $n_0(E_0)$ will strike the target $n_a = n_0$ at $E = E_m$ -- hence the name "modified shooting method." Now $\mathcal{E}(v_D)$ depends on v_D because $E_p(v_D)$ depends on v_D. Our problem is therefore simply to solve the scalar nonlinear algebraic equation

$$\mathcal{E}(v_D) = E_m - E_p(v_D) = 0 \tag{A-1}$$

This can be solved by either the Newton-Raphson or the Secant Method [11,12]. Since for each given value of v_D, $E_p(v_D)$ must be computed numerically by solving the "initial-value problem" (9a) and (9c) and then determining the value of E when $n_a = n_0$, it would usually be more efficient to use the Secant Method. To summarize, our "modified shooting method" consists of transforming the two-point boundary-value problem (9a) - (9d) into a scalar nonlinear equation where the associated nonlinear function is evaluated by solving an initial-value problem.

B. TECHNIQUE FOR AVOIDING NUMERICAL ILL-CONDITIONING

Our objective in this section is to first show that (6), (8), (9b), and (10b) are well-defined at $E = E_0 = v_1/L$ even though the numerator in each

equation tends to zero. Then we will propose a numerical method for evaluating these equations in the vicinity of $E = E_0 = v_1/L$ without causing ill-conditioning.

Observe first that (9a) and (9b) can be recast into the following form:

$$\frac{dn_a}{dE} = \frac{n_a}{(q/\varepsilon)D(E)} \frac{[v(E)-v(v_1/L)]}{n_a-n_0} + \frac{v(v_1/L)}{(q/\varepsilon)D(E)} - \frac{v_D}{(q/\varepsilon)D(E)} - \frac{n_a D'(E)}{D(E)} \qquad (A-2)$$

Now substituting $n_a = n_0$ and $E = E_0 = v_1/L$ into (A-2) and applying H'opitals Rule, we obtain

$$\left.\frac{dn_a}{dE}\right|_{E=v_1/L} = \frac{n_0}{(q/\varepsilon)D} \left\{ \frac{\left.\frac{dv(E)}{dE}\right|_{E=v_1/L}}{\left.\frac{dn_a}{dE}\right|_{E=v_1/L}} \right\} + \frac{v(v_1/L)}{(q/\varepsilon)D} - \frac{v_D}{(q/\varepsilon)D} - \frac{n_a D'}{D} \qquad (A-3)$$

If we define $X \triangleq \left.\frac{dn_a}{dE}\right|_{E=v_1/L}$, $a \triangleq \frac{n_0}{(q/\varepsilon)D} \left.\frac{dv(E)}{dE}\right|_{E=v_1/L}$, and

$b \triangleq \frac{v(v_1/L)}{(q/\varepsilon)D} - \frac{v_D}{(q/\varepsilon)D} - \frac{n_a D'}{D}$, then (A-3) reduces to a quadratic equation:

$$X^2 - bX - a = 0 \qquad (A-4)$$

Solving (A-4) for X, we obtain:

$$X = \left.\frac{dn_a}{dE}\right|_{E=v_1/L} = \frac{b+\sqrt{b^2+4a}}{2} \qquad (A-5)$$

where we have chosen the positive sign in front of the square-root sign because $dn_a/dE > 0$ at $E = v_1/L \triangleq E_0$ (see Fig. 1(b)). Hence, (9a) is defined simply by (A-5) at $E = v_1/L$.

Consider next the first integrand in (8) and (6):

$$\lim_{\substack{E\to v_1/L \\ n_a \to n_0}} \left[\frac{E-v_1/L}{n_a-n_0}\right] = \frac{\frac{dE}{dE}}{\left.\frac{dn_a}{dE}\right|_{E=v_1/L}} = \frac{1}{X} \qquad (A-6)$$

$$\lim_{\substack{E\to v_1/L \\ n_a\to n_0}} \left[\frac{v(E)-v(v_1/L)}{n_a-n_0}\right] = \frac{\left.\frac{dv(E)}{dE}\right|_{E=v_1/L}}{\left.\frac{dn_a}{dE}\right|_{E=v_1/L}} = \frac{v'(v_1/L)}{X} \tag{A-7}$$

where $X \neq 0$ is as defined by (A-5). By a similar procedure, it is easily seen that (6), (8), and (10) are well defined at $E = v_1/L$.

Even though all equations are well defined at $E = v_1/L$, numerical ill-conditioning may occur unless special subroutines are included for evaluating the expressions in (6), (8), (9), and (10) at $E = v_1/L$. For example, (A-5), (A-6), and (A-7) may be used whenever $E = v_1/L$. Also, instead of using the initial condition $n_a(v_1/L) = n_0$, we can use

$$n_a\left(\frac{v_1}{L}+\delta\right) \cong n_0 + \left.\frac{dn_a}{dE}\right|_{E=v_1/L} \cdot \delta = n_0 + X\delta \tag{A-8}$$

for sufficiently small δ.

REFERENCES

1. Bulman, P. J., Hobson, G. S., and Taylor, B. C., Transferred-electron Devices, Academic Press, New York, 1972.
2. Hartnagel, H. L., Gunn-effect Logic Devices, Heinemann Educational Books, London, 1973.
3. Hobson, G. S., The Gunn Effect, Clarendon Press, Oxford, 1974.
4. Howes, M. J. and Morgan, D. V., Microwave Devices, John Wiley and Sons, New York, 1976.
5. Carroll, J. E. and Giblin, R. A., "A Low Frequency Analog for a Gunn-Effects Oscillator," IEEE Trans. on Electron Devices, Vol. ED-14, No. 10, October 1967, pp. 640-656.
6. Robrock, R. B., II, "A Lumped Model for Characterizing Single and Multiple Domain Propagation in Bulk GaAs," IEEE Trans. on Electron Devices, Vol. ED-17, No. 2, February 1970, pp. 93-102.
7. Gunshor, R. L. and Kak, A. C., "Lumped-Circuit Representation of Gunn Diodes in Domain Mode," IEEE Trans. on Electron Devices, Vol. ED-19, No. 6, June 1972, pp. 765-770.
8. Kak, A. C. and Gunshor, R. L., "The Transient Behavior of High-Field Dipole Domains in Transferred Electron Devices," IEEE Trans. on Electron Devices, vol. ED-20, No. 1, January 1973, pp. 1-5.
9. Butcher, P. N., Fawcett, W., and Ogg, N. R., "Field-Dependent Diffusion on Stable Domain Propagation in the Gunn Effect," Brit. J. Appl. Phys., Vol. 18, 1967, pp. 755-759.
10. Sze, S. M., Physics of Semiconductor Devices, J. Wiley, New York, 1969.
11. Dahlquist, G. and Bjorck, A., Numerical Methods, Prentice-Hall, Englewood Cliffs, N. J., 1974.
12. Chua, L. O. and Lin, P. M., Computer-Aided Analysis of Electronic Circuits: Algorithms and Computational Techniques, Prentice-Hall, Englewood Cliffs, N. J., 1975.
13. Kurokawa, K., "Transient Behavior of High-Field Domains in Bulk Semiconductors," Proc. of the IEEE, Vol. 55, September 1967, pp. 1615-1616.
14. Butcher, P. N., Fawcett, W. and Hilsam, C., "A Simple Analysis of Stable Domain Propagation in the Gunn Effect," Brit. J. Appl. Phys., Vol. 17, 1966, pp. 841-850.

15. Desoer, C. A., Notes for a Second Course on Linear Systems, Van Nostrand Reinhold, New York, 1970.

16. Chua, L. O., Introduction to Nonlinear Network Theory, McGraw-Hill, New York, 1969.

17. Hirsch, M. W. and Smale, S., Differential Equations, Dynamical Systems, and Linear Algebra, Academic Press, New York, 1974.

FIGURE CAPTIONS

Fig. 1. (a) A one-dimensional Gunn diode of cross-sectional area A and length L.
(b) Carrier Concentration at one instant of time showing a dipole being formed with an accumulation layer from x_1 to x_3, and a depletion layer from x_3 to x_2. Electron density n in the accumulation layer is denoted by n_a and that in the depletion layer is denoted by n_d.
(c) A high-field domain being formed at the same instant of time. The domain is assumed to increase monotonically over the interval $[x_1,x_3]$ from E_0 to E_m, and then decrease monotonically over the interval $[x_3,x_2]$ from E_m to E_0.

Fig. 2. The general circuit model for simulating the dynamics of the domain formation in a Gunn diode having an n_0L product greater than 10^{12} cm^{-2}. The function $F(v_1,v_2)$ is given by Equation (6).

Fig. 3. Complete Gunn diode circuit model which includes domain nucleation, formation, and extinction phenomena. The three controlled resistors $R_1(v_1)$, $R_2(v_2)$, and $R_3(v_3)$ depend on v_1, v_2, and v_3, respectively, as given by Equations (51), (52), and (53). These resistors behave like relays and therefore should be described by a separate subroutine using logic statements to save computer time.

Fig. 4. Complete Gunn diode circuit model for the zero-diffusion case. The nonlinear resistor R and the linear capacitor C_1 are as described in Fig. 3. The controlled current source coefficient is given by the simplified expression:

$$I_D = \int_{v_1/L}^{(v_1/L)+\sqrt{(2qn_0/\varepsilon)v_2}} [v(v_1/L)-v(E)]dE - I$$

The three controlled resistors are described Equations (51), (52), and (53). The dotted lines show the controlling variables.

Fig. 5. A single-cavity Gunn-diode circuit and the external circuit parameters leading to four distinct modes of steady-state operation.

Fig. 6. The waveforms associated with the Gunn-diode circuit operating under the transit-time mode. Horizontal scale is 57×10^{-12} seconds per division. Voltage normalization constant = 4 volts.

Fig. 7. The normalized terminal voltage and current waveforms of the Gunn-diode circuit operating under the transit-time mode and its associated "ac" $\bar{I} - \bar{V}$ curve. Voltage normalization constant = 4 volts, current normalization constant = 0.512 mA.

Fig. 8. The waveforms associated with the Gunn-diode circuit operating under the delayed-domain mode. Horizontal scale is 75×10^{-12} seconds per division. Voltage normalization constant = 4 volts.

Fig. 9. The normalized terminal voltage and current waveforms of the Gunn-diode circuit operating under the delayed-domain mode and its associated "ac" $\bar{I} - \bar{V}$ curve. Voltage-normalization constant = 4 volts, current normalization constant = 0.512 mA.

Fig. 10. The waveforms associated with the Gunn-diode circuit operating under the quenched-domain mode. Horizontal scale is 44×10^{-12} seconds per division. Voltage normalization constant = 4 volts.

Fig. 11. The normalized terminal voltage and current waveforms of the Gunn-diode circuit operating under the quenched-domain mode. Voltage normalization constant = 4 volts, current normalization constant = 0.512 mA.

Fig. 12. The waveforms associated with the Gunn-diode circuit operating under the LSA mode. Horizontal scale is 0.33×10^{-12} seconds per division. Voltage normalization constant = 4 volts.

Fig. 13. The normalized terminal voltage and current waveforms of the Gunn-diode circuit operating under the LSA mode, and its associated "ac" $\bar{I} - \bar{V}$ curve. Votlage normalization constant = 4 volts, current normalization constant = 0.512 mA.

Fig. 14. A two-Gunn-diode AND logic gate circuit and its output transient response $v_0(t)$ due to two unsymmetrical square-wave inputs $v_{s_1}(t)$ and $v_{s_2}(t)$. Horizontal scale is 1.4×10^{-12} seconds per division. Voltage normalization constant = 4 volts.

Fig. 15. The "dc" $\bar{I} - \bar{V}$ curve associated with a Gunn diode and its associated equilibrium points.

Fig. 16. A geometrical interpretation of the shooting method.

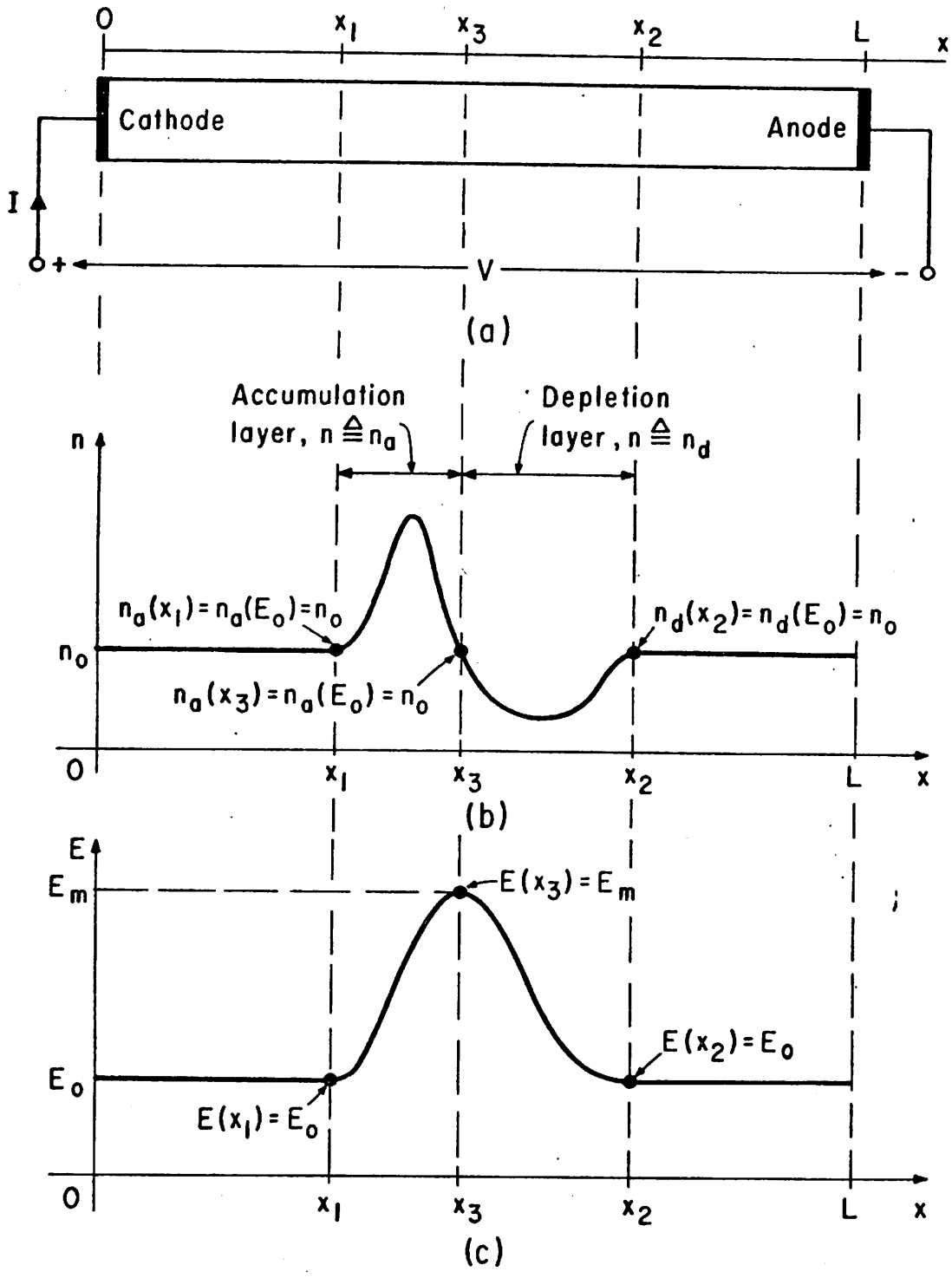
0
x_1
x_3
x_2
L
x
Cathode
Anode
I
+
V
-
(a)
Accumulation layer, $n \triangleq n_a$
Depletion layer, $n \triangleq n_d$
n
$n_a(x_1) = n_a(E_0) = n_0$
$n_d(x_2) = n_d(E_0) = n_0$
n_0
$n_a(x_3) = n_a(E_0) = n_0$
0
x_1
x_3
x_2
L
x
(b)
E
E_m
$E(x_3) = E_m$
$E(x_2) = E_0$
E_0
$E(x_1) = E_0$
0
x_1
x_3
x_2
L
x
(c)

Fig. 1.

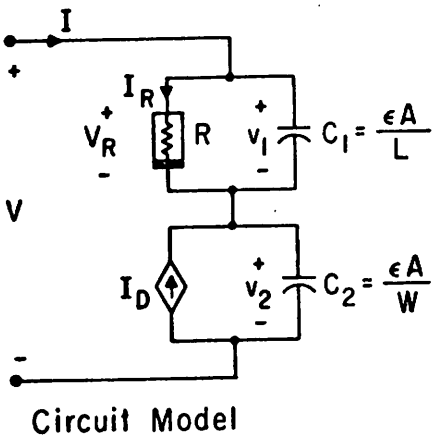

Circuit Model

Nonlinear Resistor R:

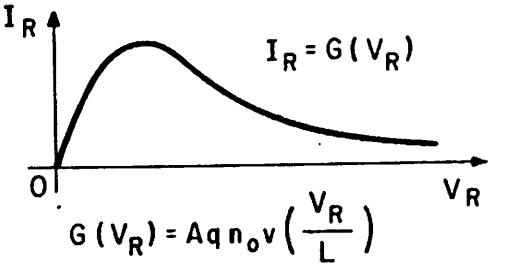

$$G(V_R) = Aq n_o v \left(\frac{V_R}{L}\right)$$

Nonlinear Controlled Current Source:

$$I_D = C_2 F(v_1, v_2) - I \triangleq I_D(v_1, v_2, I)$$

Fig. 2.

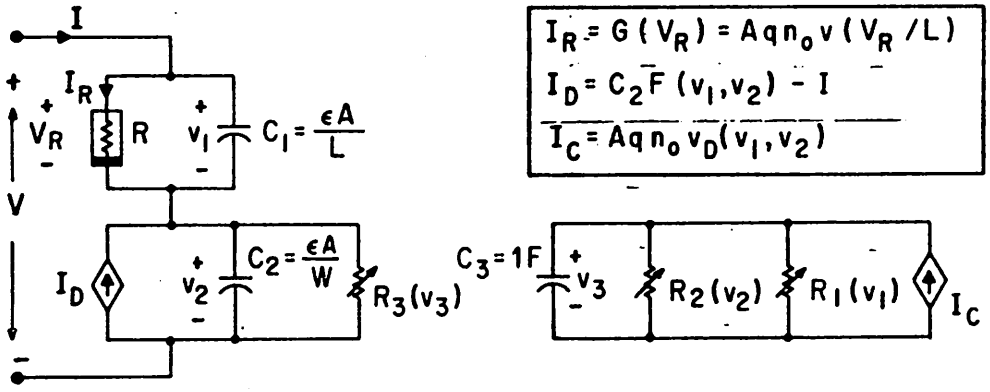
I
+
V
−
I_R
V_R
R
v_1
$C_1 = \frac{\epsilon A}{L}$
I_D
v_2
$C_2 = \frac{\epsilon A}{W}$
$R_3(v_3)$
$C_3 = 1F$
v_3
$R_2(v_2)$
$R_1(v_1)$
I_C
$I_R = G(V_R) = Aqn_o v(V_R/L)$
$I_D = C_2 F(v_1, v_2) - I$
$I_C = Aqn_o v_D(v_1, v_2)$

Fig. 3.

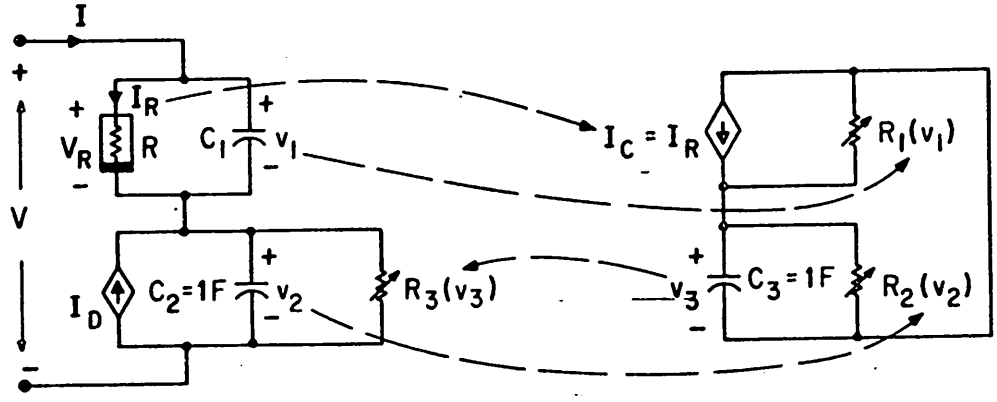
I
+
V
−
I_R
V_R
R
C_1
v_1
I_D
$C_2 = 1F$
v_2
$R_3(v_3)$
$I_C = I_R$
$R_1(v_1)$
v_3
$C_3 = 1F$
$R_2(v_2)$

Fig. 4.

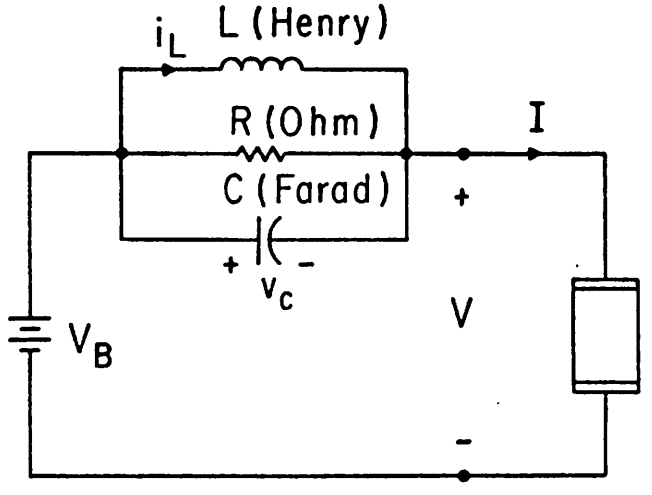

Gunn Diode Circuit Model Parameters:

$n_0 = 1 \times 10^{16} cm^{-3}$, $L = 10 \mu m$

$A = 1 \mu m^2$, $q = 1.602 \times 10^{-19}$ Coulomb

$C_1 = 1.16 \times 10^{-17}$ Farad, $C_2 = 1$ Farad

$$I_R = G(V_R) = 1.6 \times 10^{-11} \times \left\{ \frac{8 \times 10^6 V_R + 3.125 \times 10^4 V_R^4}{1 + 3.9 \times 10^{-3} V_R^4} \right\}$$

(a)

Operating Mode	R	L	C	V_B
Transit-Time	1	0.5×10^{-10}	1×10^{-12}	4.8
Delayed-Domain	100×10^6	2×10^{-13}	0.5×10^{-8}	4.8
Quenched-Domain	100×10^6	0.5×10^{-12}	1×10^{-9}	4.8
LSA	100×10^6	1×10^{-13}	1×10^{-13}	4.8

(b)

Fig. 5.

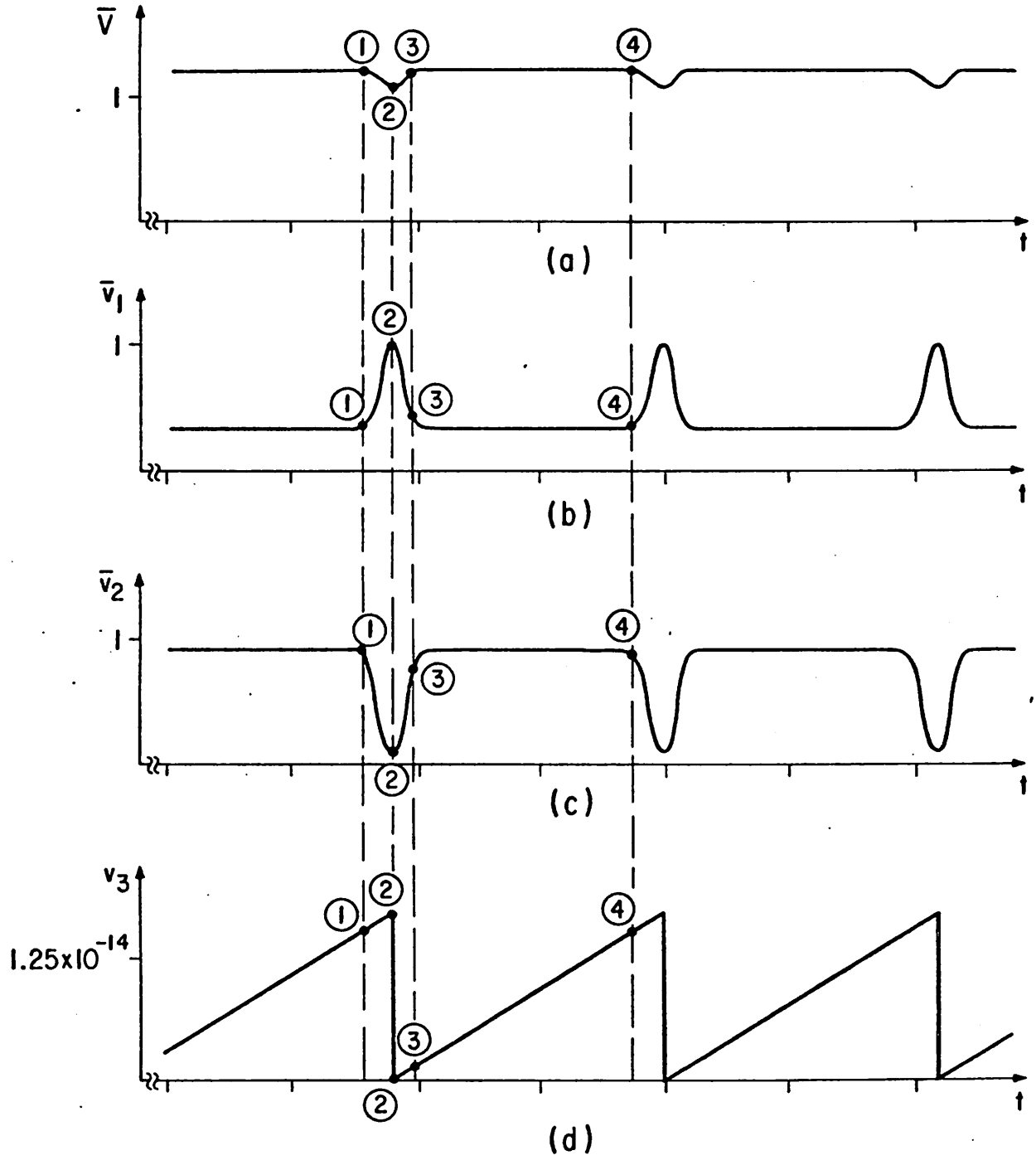
$\bar{V}$
1
①
②
③
④
t
(a)
$\bar{v}_1$
1
①
②
③
④
t
(b)
$\bar{v}_2$
1
①
②
③
④
t
(c)
v_3
1.25×10^{-14}
①
②
③
④
t
(d)

Fig. 6.

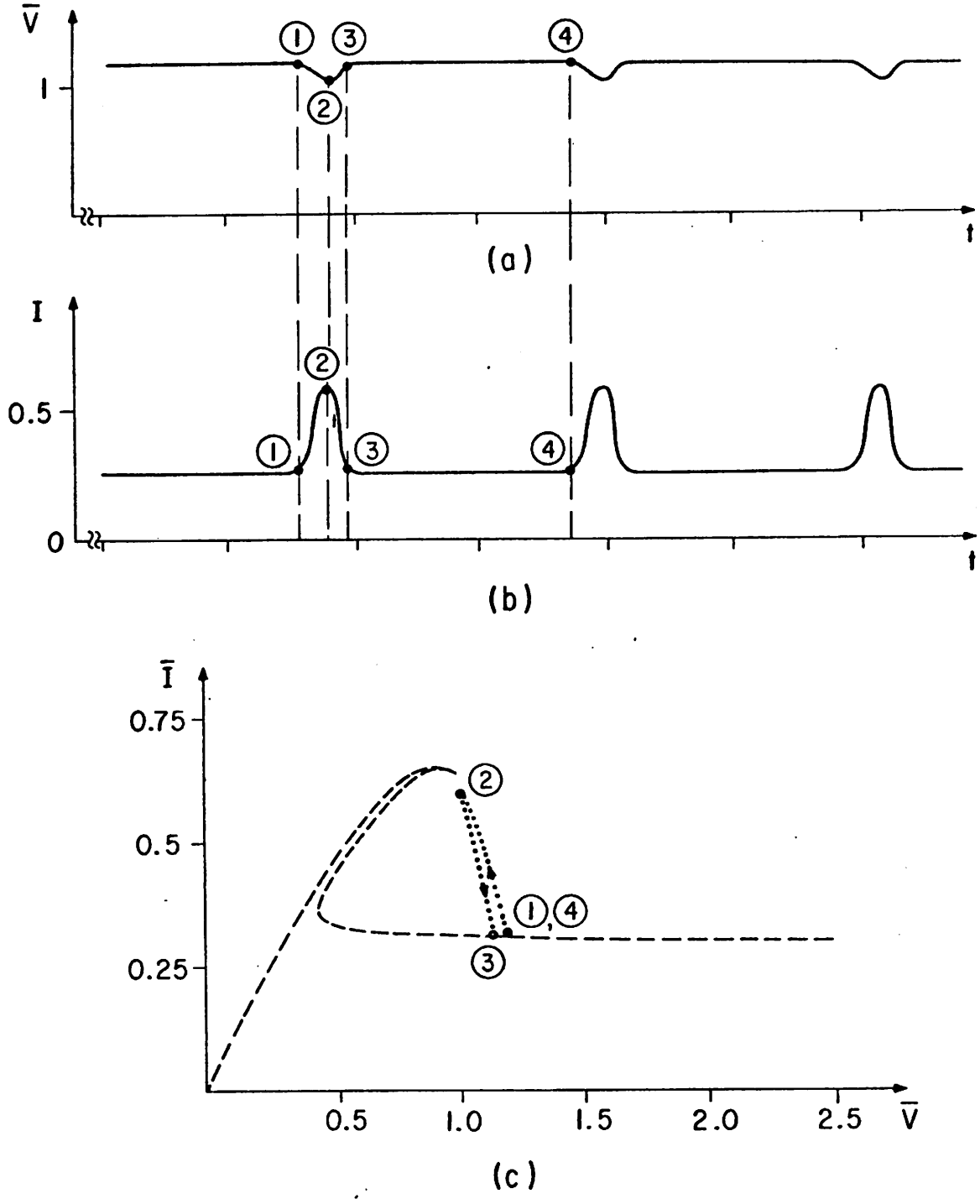

Fig. 7.

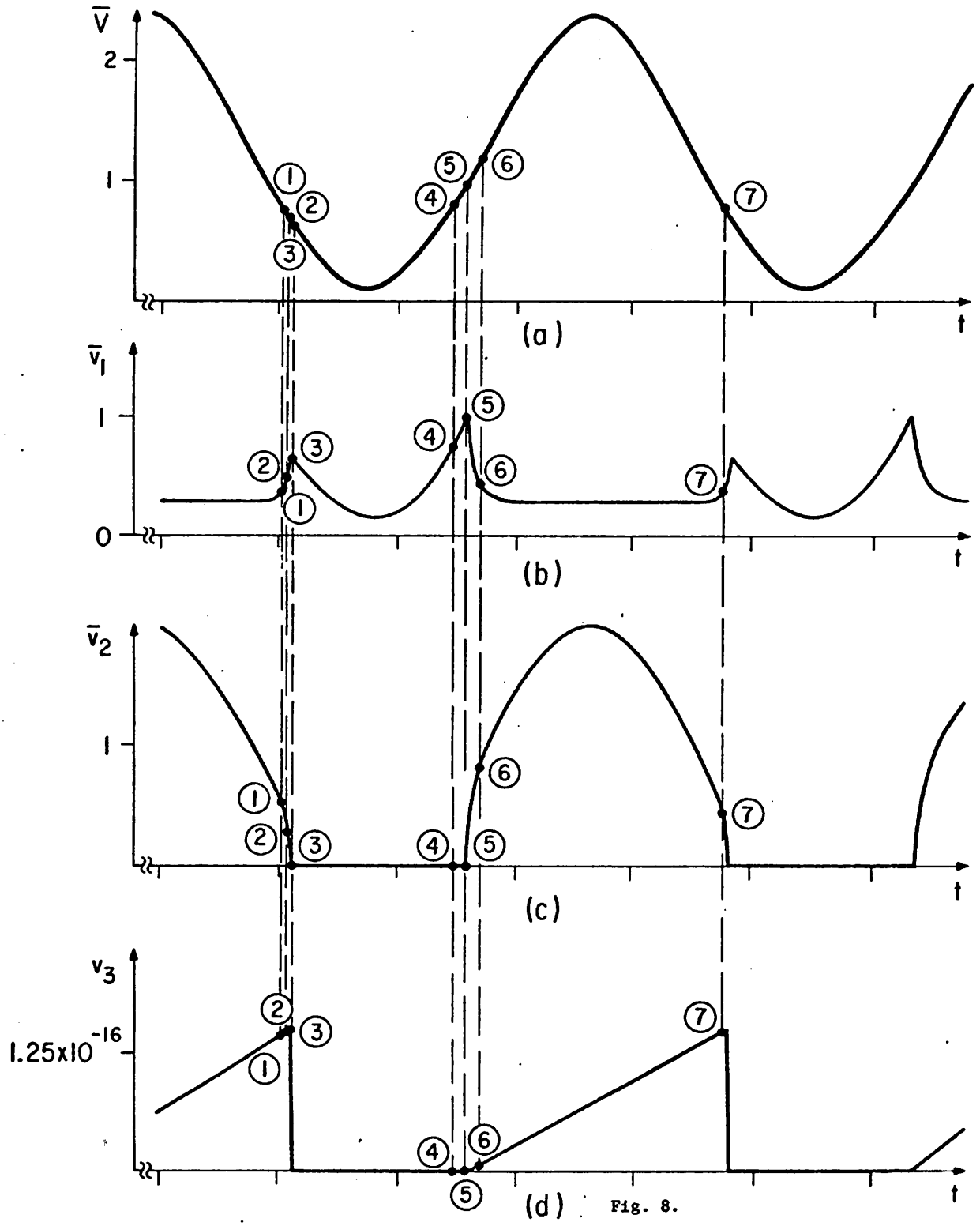

Fig. 8.

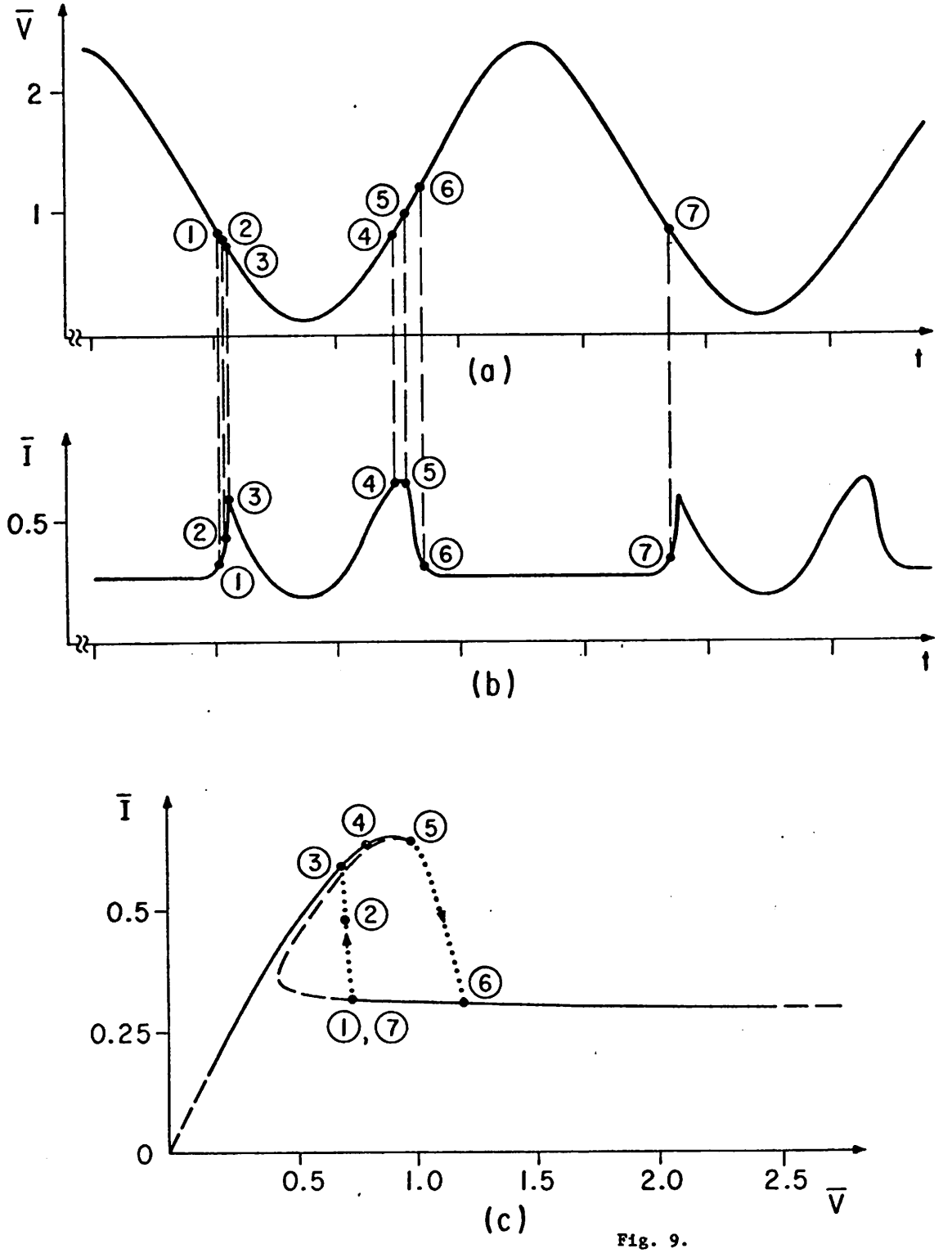

Fig. 9.

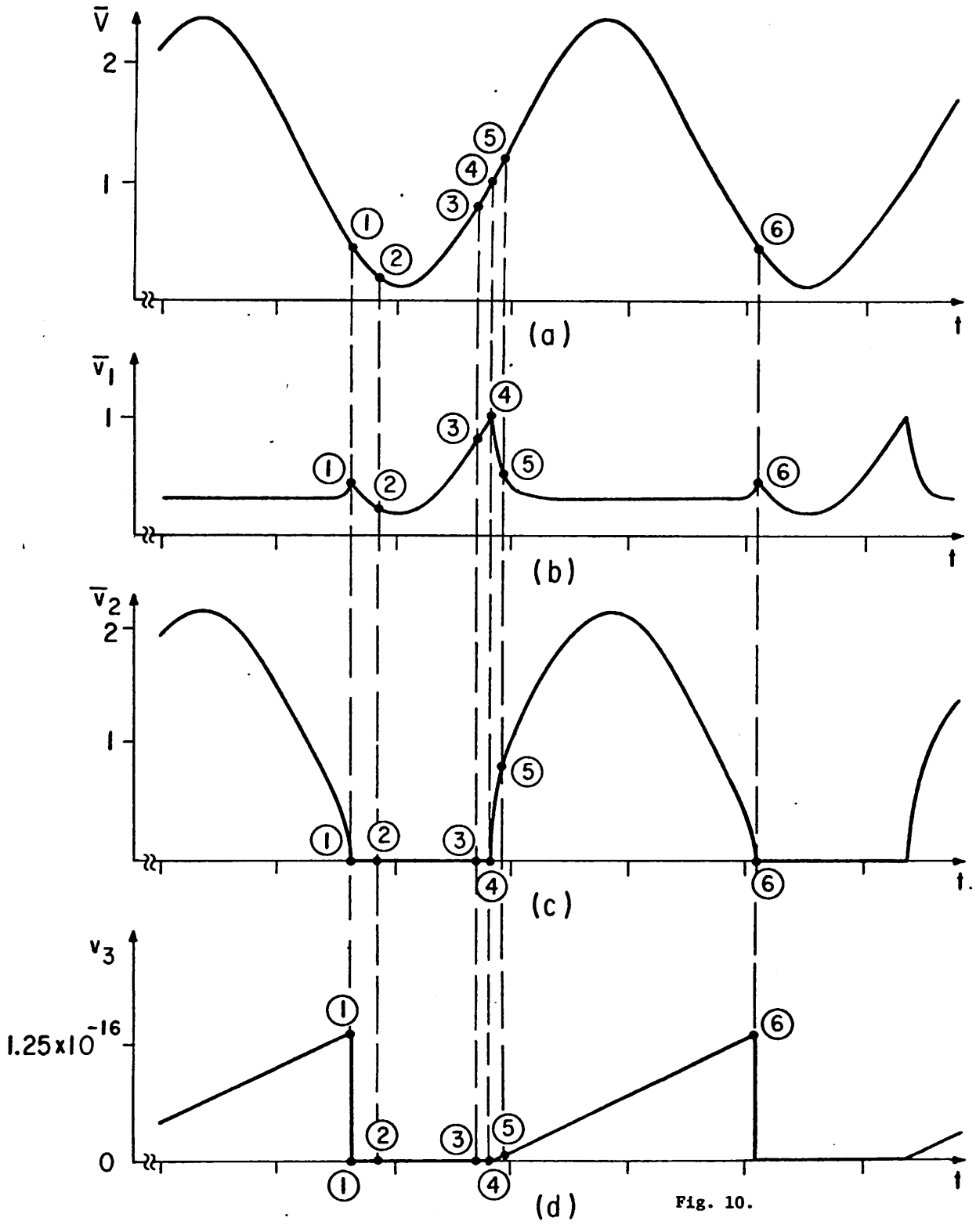

Fig. 10.

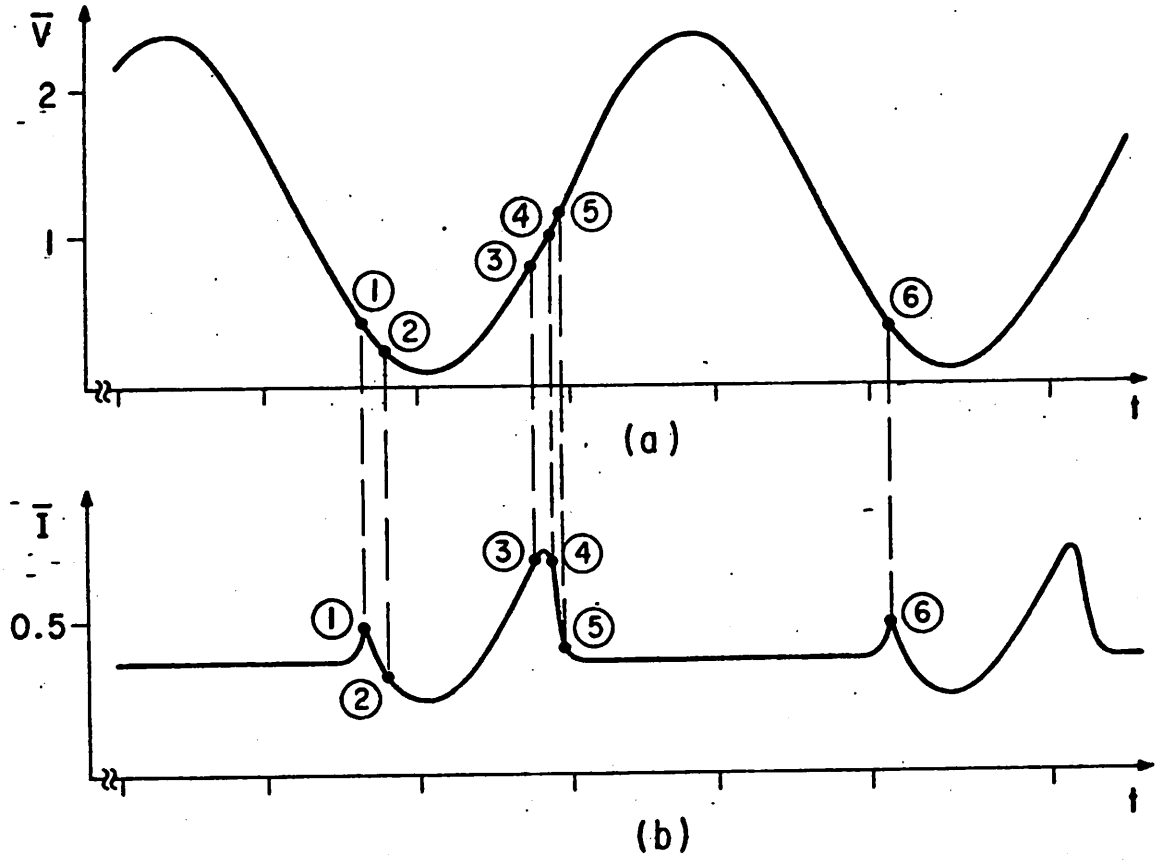

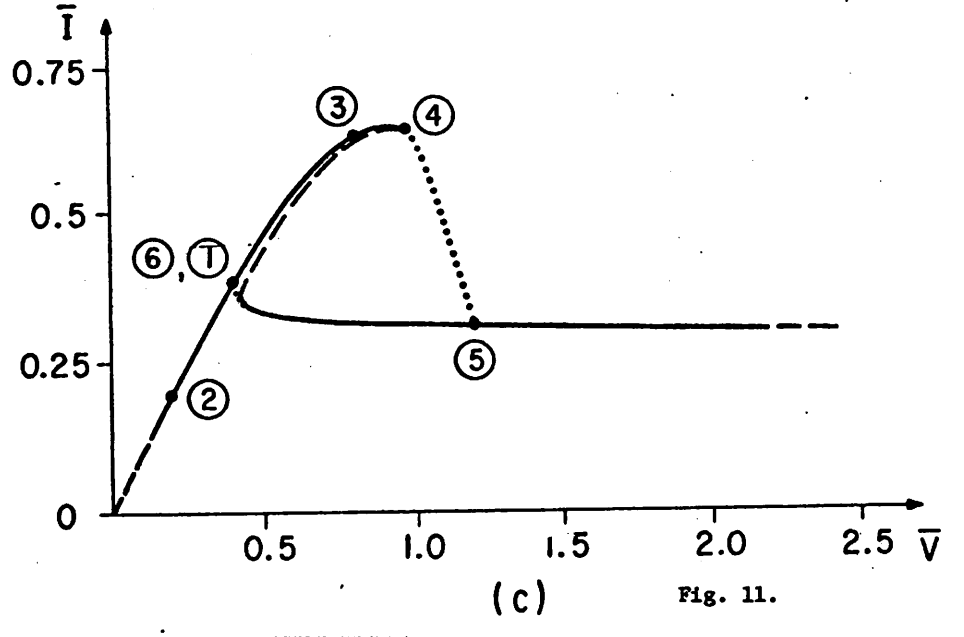

Fig. 11.

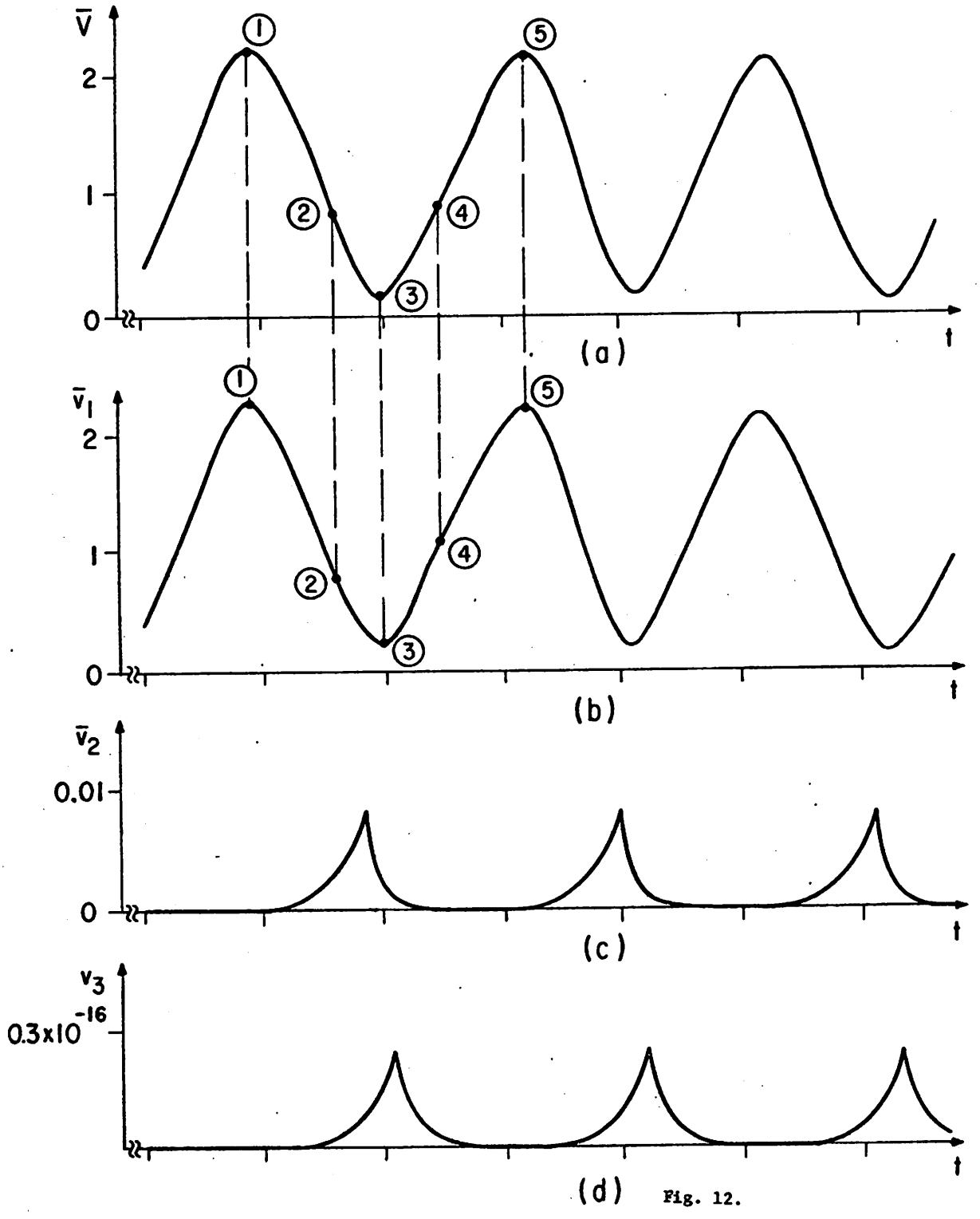

Fig. 12.

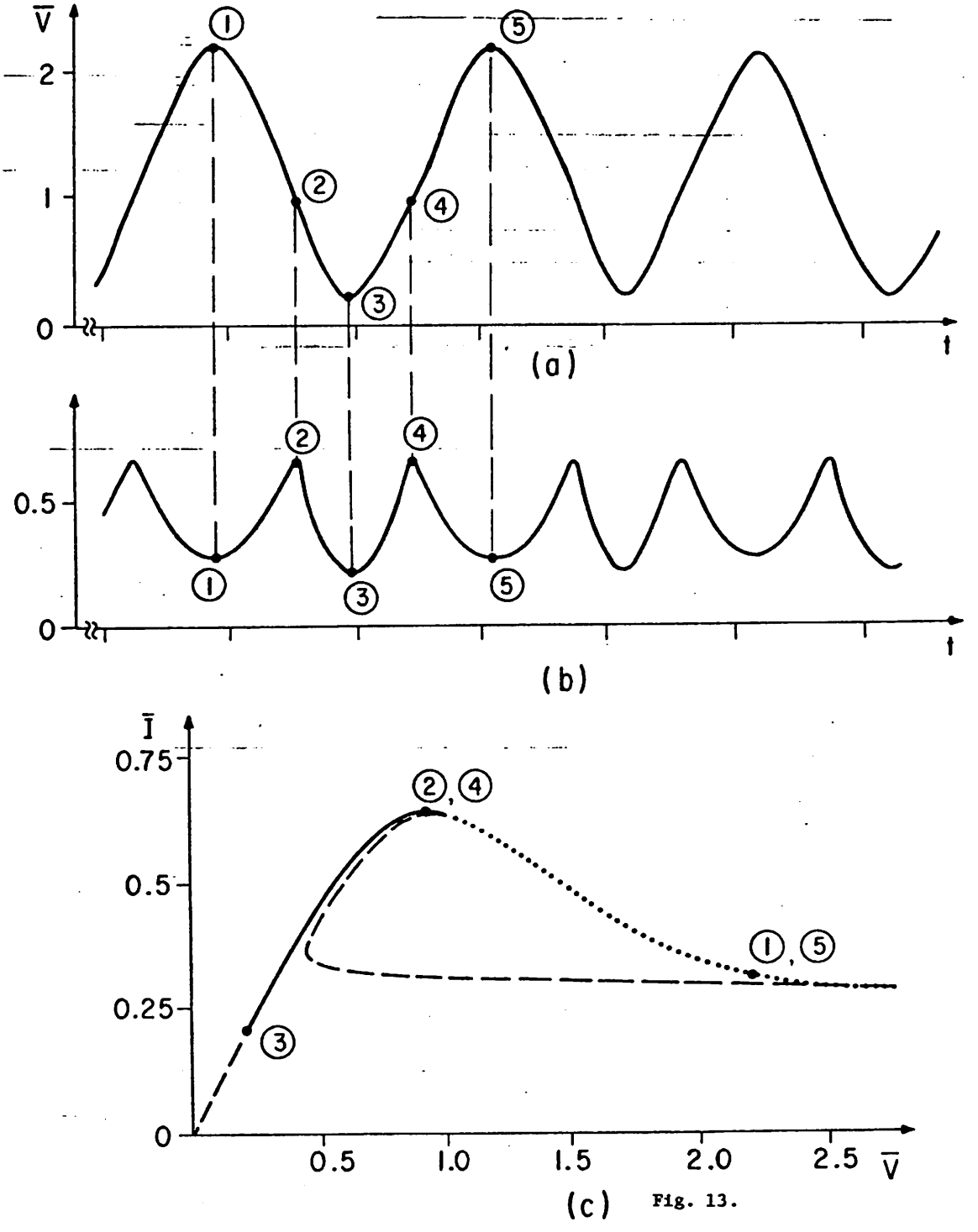

Fig. 13.

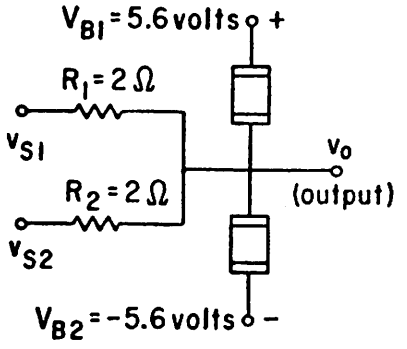

AND GATE LOGIC OPERATION

Polarity of Input Signal		Polarity of Output Signals	Type of Binary Signal
v_{S1}	v_{S2}		
+	+	+	ON
+	−	−	OFF
−	+	−	OFF
−	−	−	OFF

(a)

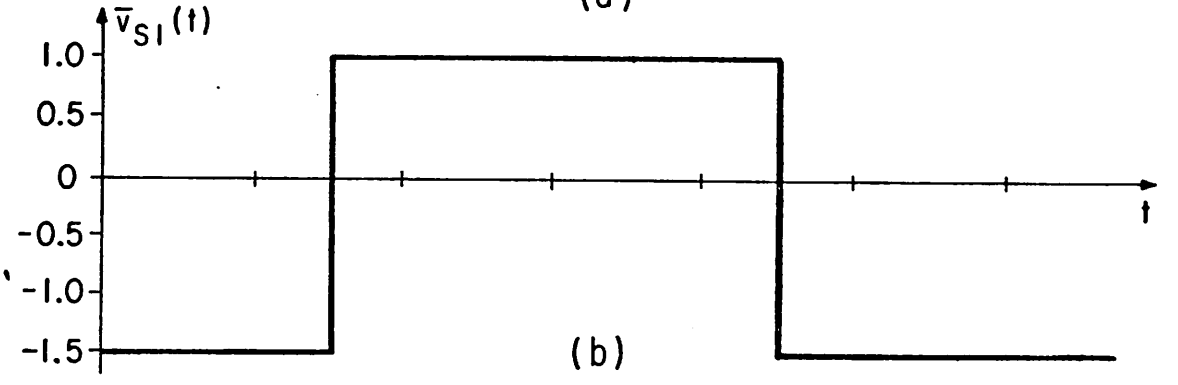

(b)

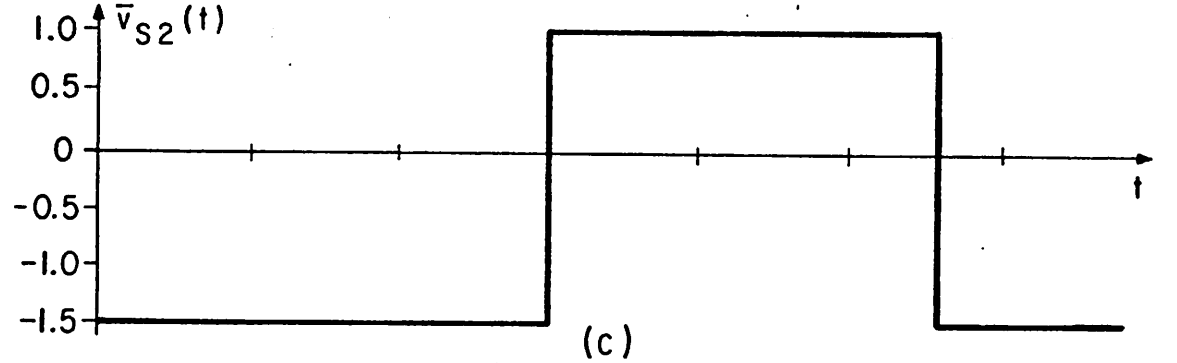

(c)

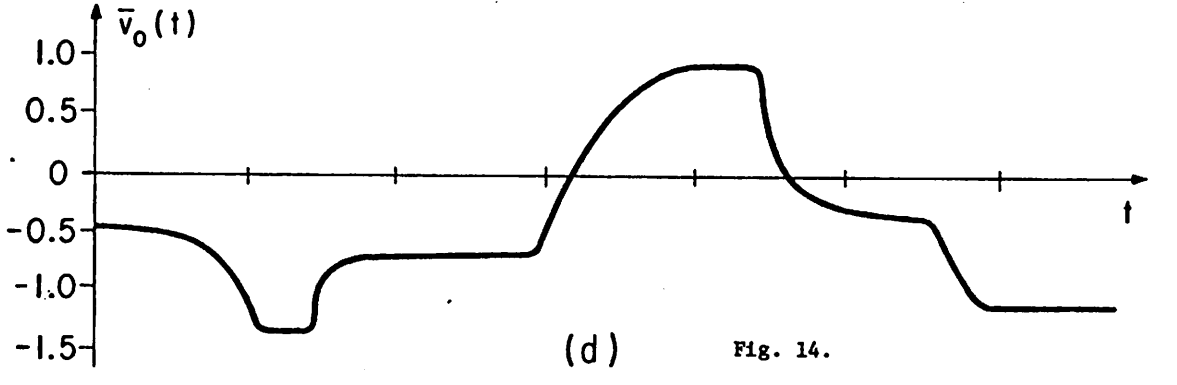

(d)

Fig. 14.

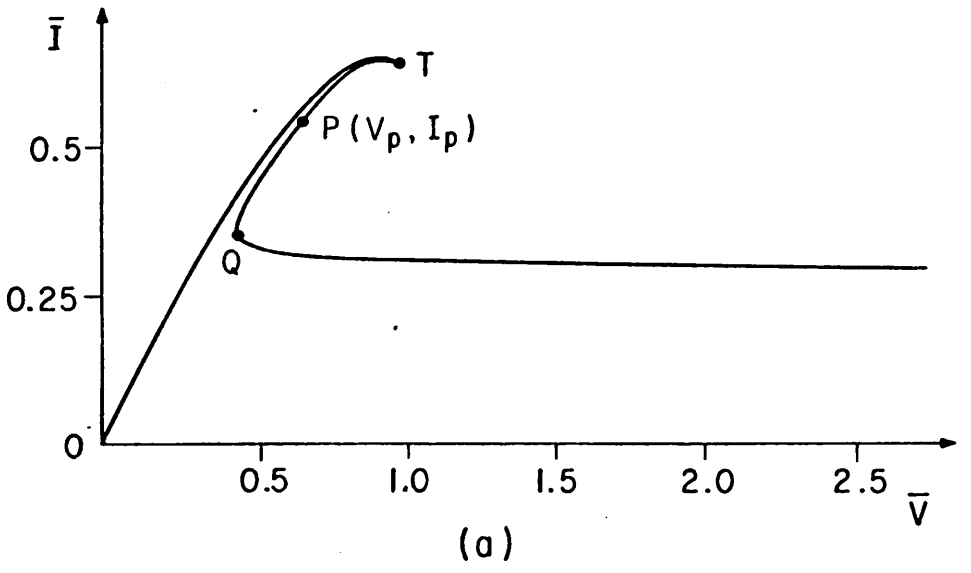
Ī
0.5
0.25
0
T
P (Vp, Ip)
Q
0.5
1.0
1.5
2.0
2.5
V̄

(a)

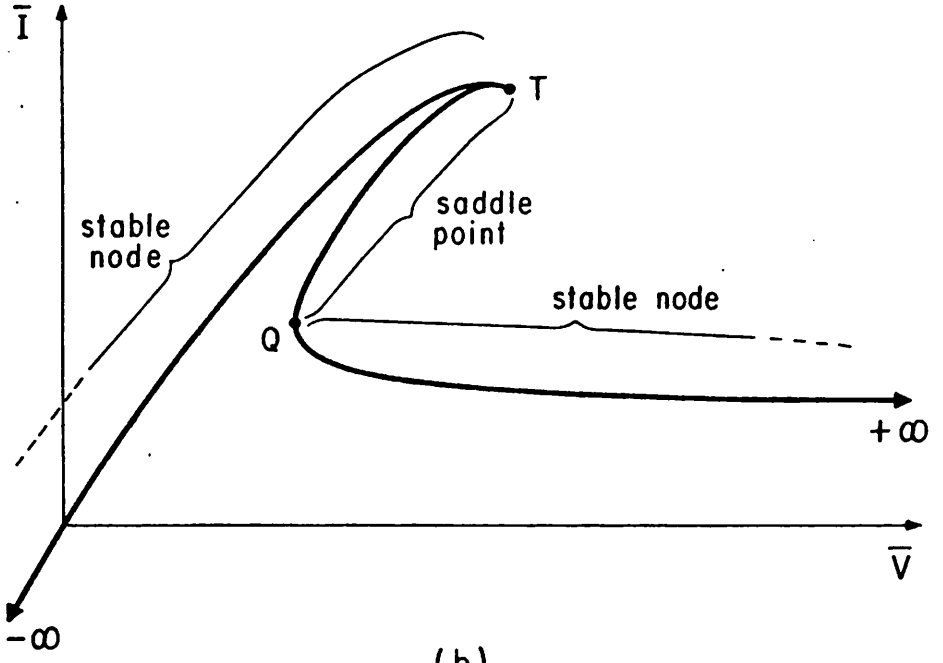
Ī
T
stable
node
saddle
point
stable node
Q
+∞
V̄
−∞

(b)

Fig. 15.

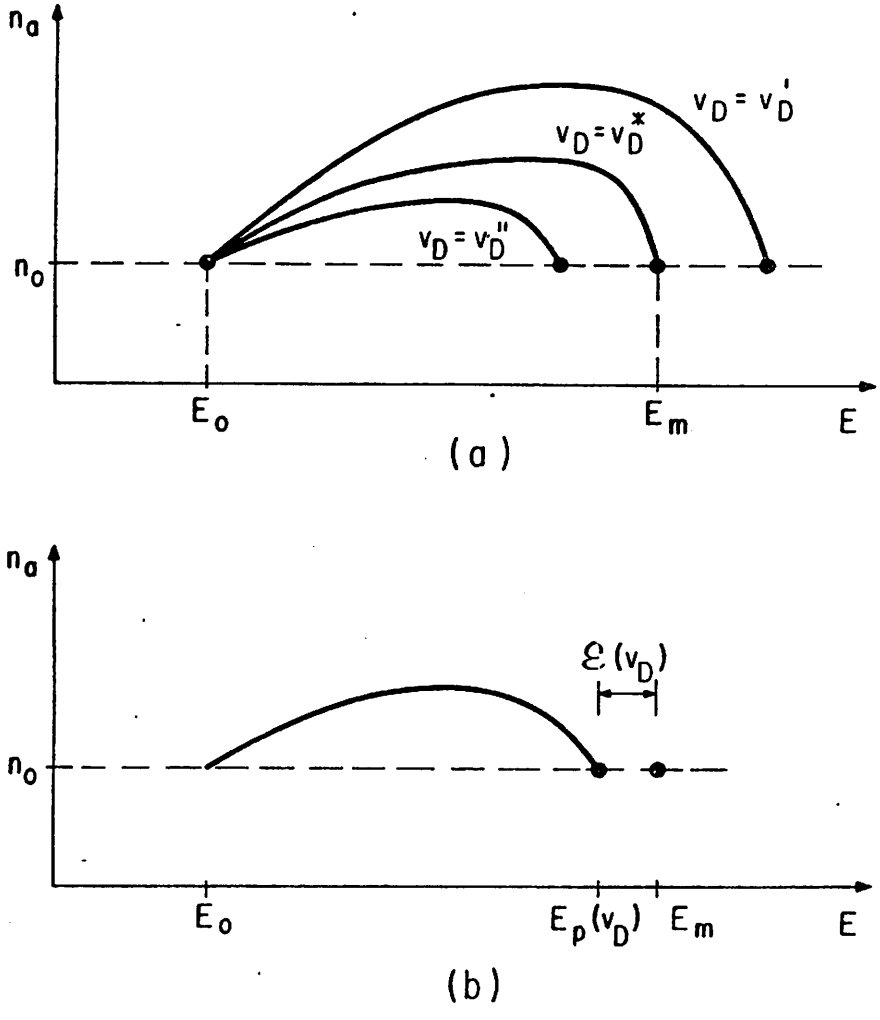

Fig. 16.